KfK 2838
Dezember 1979
(1. Ex.)

Elastic Scattering of 104 MeV Alpha Particles from ^{40,42,44,48}Ca and Determination of the Optical Potentials

H. J. Gils, E. Friedman, H. Rebel, J. Buschmann, S. Zagromski,
H. Klewe-Nebenius, B. Neumann, R. Pesl, G. Bechtold
Institut für Angewandte Kernphysik

Kernforschungszentrum Karlsruhe

KERNFORSCHUNGSZENTRUM KARLSRUHE

Institut für Angewandte Kernphysik

KfK 2838

Elastic Scattering of 104 MeV Alpha Particles from $^{40,42,44,48}Ca$ and Determination of the Optical Potentials

H.J. Gils, E. Friedman[+], H. Rebel, J. Buschmann
S. Zagromski, H. Klewe-Nebenius[++], B. Neumann,
R. Pesl and G. Bechtold

[+] The Racah Institute of Physics, The Hebrew University, Jerusalem, Israel

[++] Kernforschungszentrum Karlsruhe GmbH, Institut für Radiochemie

Kernforschungszentrum Karlsruhe GmbH, Karlsruhe

Kernforschungszentrum Karlsruhe GmbH
ISSN 0303-4003

Abstract

Differential cross sections for elastic scattering of 104 MeV α particles from $^{40, 42, 44, 48}$Ca have been measured with high angular accuracy over a wide angular range. Optical model analyses using different approaches for the potential form including a Fourier-Bessel description of the real potential reveal isotopic differences which, in particular for ^{48}Ca, indicate a small neutron skin. The model dependence of the extracted quantities is discussed in detail.

Elastische Streuung von 104 MeV α-Teilchen an $^{40, 42, 44, 48}$Ca und Bestimmung der Optischen Potentiale

Zusammenfassung

Differentielle Wirkungsquerschnitte der elastischen Streuung von 104 MeV α-Teilchen an $^{40, 42, 44, 48}$Ca wurden mit hoher Winkelgenauigkeit gemessen. Analysen mit dem Optischen Modell unter Benutzung der Fourier-Bessel-Beschreibung des reellen Potentials ergeben Differenzen der Potentiale zwischen den einzelnen Isotopen, die - insbesondere für ^{48}Ca - die Existenz einer schmalen Neutronenhaut an der Kernoberfläche anzeigen. Die Modellabhängigkeit der gewonnenen Potentiale wird eingehend diskutiert.

1. INTRODUCTION

One of the most important tests of current theories of nuclear structure is provided by investigations of the shape of the nucleon distributions. In general, however, the m a t t e r distribution of nuclei is less accessible experimentally than the nuclear c h a r g e distribution. The elastic scattering of strongly interacting particles has been suggested as a source of information on nuclear matter distributions. Due to the insufficient knowledge of the strong interaction, hadronic probes always imply the use of a model, either in an explicit or implicit form, when going from the phenomenologically observed interaction to the nucleon density distribution. Obviously the problem may be split into two parts: (i) How accurately can the phenomenological interaction potential between a probe particle and a target nucleus be determined? (ii) How reliable is the interpretation in terms of the nuclear density distributions? In addressing these questions the scattering of α particles in the 100 MeV energy region appears to be a most attractive method. In this energy region α particle scattering shows not only the well-known diffraction phenomena, which are characteristic of the absorption at the nuclear surface, but also a finite transparency of the nuclear interior due to the refractive property of the real potential.

As shown by Goldberg et al.[1] the α particle-nucleus optical potential can be determined with a high degree of uniqueness if the range of the observed angular distribution extends beyond the "nuclear rainbow angle", which reflects sensitivity to the real potential at small radii. When the constraints due to the choice of a specific functional form for the real optical potential are removed by introducing more flexible methods[2] (which correspond to the "model-indepedent" techniques in electron scattering analyses) one should be able to obtain reliable and accurate interaction potentials from sufficiently precise experimental data. The case of scattering on calcium isotopes is of particular interest. We find here not only an isotopic sequence ranging to a large neutron excess in ^{48}Ca and including two subsequent shell closures, but also a considerable amount of theoretical results and experimental information from other sources which may help to understand the connection between the optical potentials and the nuclear density distributions.

In this paper we report the results of precision measurements of the elastic scattering of 104 MeV α particles by $^{40,42,44,48}Ca$. The measured differential cross sections extend over a wide angular range and include the "nuclear rainbow" region as well as exceptionally small angles in order to increase the sensitivity also to the surface region. The analysis of the experimental data aims primarily at the determination of the strength and shape of the optical potentials, a good knowledge of which is a prerequisite for any further discussion of nuclear density distributions. In particular, the model dependence of the derived potentials which results from the use of simple functional forms is greatly reduced by applying the Fourier-Bessel (FB) method[2]. As compared to the conventional approaches the FB method is capable of revealing small isotopic differences in the interaction potentials and yield better descriptions of the differential cross sections. Additionally, it provides realistic estimates of the uncertainties of the various extracted quantities. A preliminary account of part of the present results (for $^{40,48}Ca$) was already published[3]. A further analysis of the present results in terms of the nuclear density distributions of the calcium isotopes invoking a density dependent folding model is the topic of another paper[4].

2. EXPERIMENTAL

The experiments on $^{40, 42, 44, 48}Ca$ were performed at the scattering facility of the Karlsruhe Isochronous Cyclotron[5] using 104 MeV α particles. The targets were self-supporting metal foils of natural Ca (96.9 % ^{40}Ca) and highly enriched $^{42,44,48}Ca$ (enrichment 94-99 %). The target thicknesses ranged between 1 and 5 mg/cm^2. The α particle beam was monochromized to about 50 keV FWHM and focussed to a beam spot of about 1.5 mm diameter at the target position. From the emittance of the cyclotron the angular divergence of the beam (80 % intensity) was estimated to be less than 0.20^0. The scattering chamber used had a diameter of 130 cm enabling to obtain a small angular acceptance of $\sim 0.15^0$ with 1.5 mm slits in front of the detectors; thus excessive slit scattering was avoided. The scattered α particles were detected by four Si surface barrier detectors of 4 mm thickness mounted on a movable arm with angular distances of 1.5^0 between each other. The electronical set up consisted of standard

NIM-modules and a data acquisition system based on a NOVA II computer. The overall energy resolution of 150-180 keV (FWHM) was sufficient to separate inelastic and contaminant peaks (C,O) at almost all scattering angles. Particle identification was not necessary because the maximum energy loss of protons, deuterons and tritons in the detectors was less than 33 MeV, far outside the energy region of elastically scattered α particles. ^{3}He particles do not interfere with the spectra because of the distinctly different Q values (about 15 MeV) compared to α particles. Great efforts were focussed on the determination of the absolute zero point of the scattering angle by measuring on both sides of the beam (left-right-measurement) and additionally by observing the kinematical behavior of the carbon and oxygen target contamination peaks. The total uncertainty of the scattering angles was determined to be $\pm\ 0.05^{0}$. At each scattering angle the four targets were measured in turn in order to avoid angular errors by new settings. The elastic scattering cross sections were measured from $\Theta_{CM} = 3^{0}$ up to $\Theta_{CM} = 110^{0}$ in steps of 0.5^{0} in the diffraction region ($\Theta_{CM} \lesssim 60^{0}$) and in steps of 1.5^{0} beyond. The beam current was measured by a Faraday cup behind the scattering chamber and additionally monitored by a fixed angle detector. The statistical errors were 1-2 % at most of the forward angles. The uncertainty of the absolute scattering angle was converted into cross section errors by taking into account the slope of the angular distributions.

Since the uncertainties of target thickness, integrated beam current and detector acceptance determined the absolute scale of the cross sections only within 10 % accuracy the data were finally normalized at forward angles to optical model predictions. The experimental results cover nine orders of magnitude as displayed in Fig. 1. With increasing mass number one observes an increasing shift of the diffraction minima towards smaller angles. The behavior of the cross sections in the transition region between diffraction and refraction and also the decrease at large angles are very similar for ^{40,42,44}Ca whereas the transition structure and the slope of the refractive decrease in the case of ^{48}Ca slightly differ from those of the other isotopes. The measurements for ^{40}Ca and ^{48}Ca had been repeated over a period of one year with excellent reproducibility of the results within 1 %.

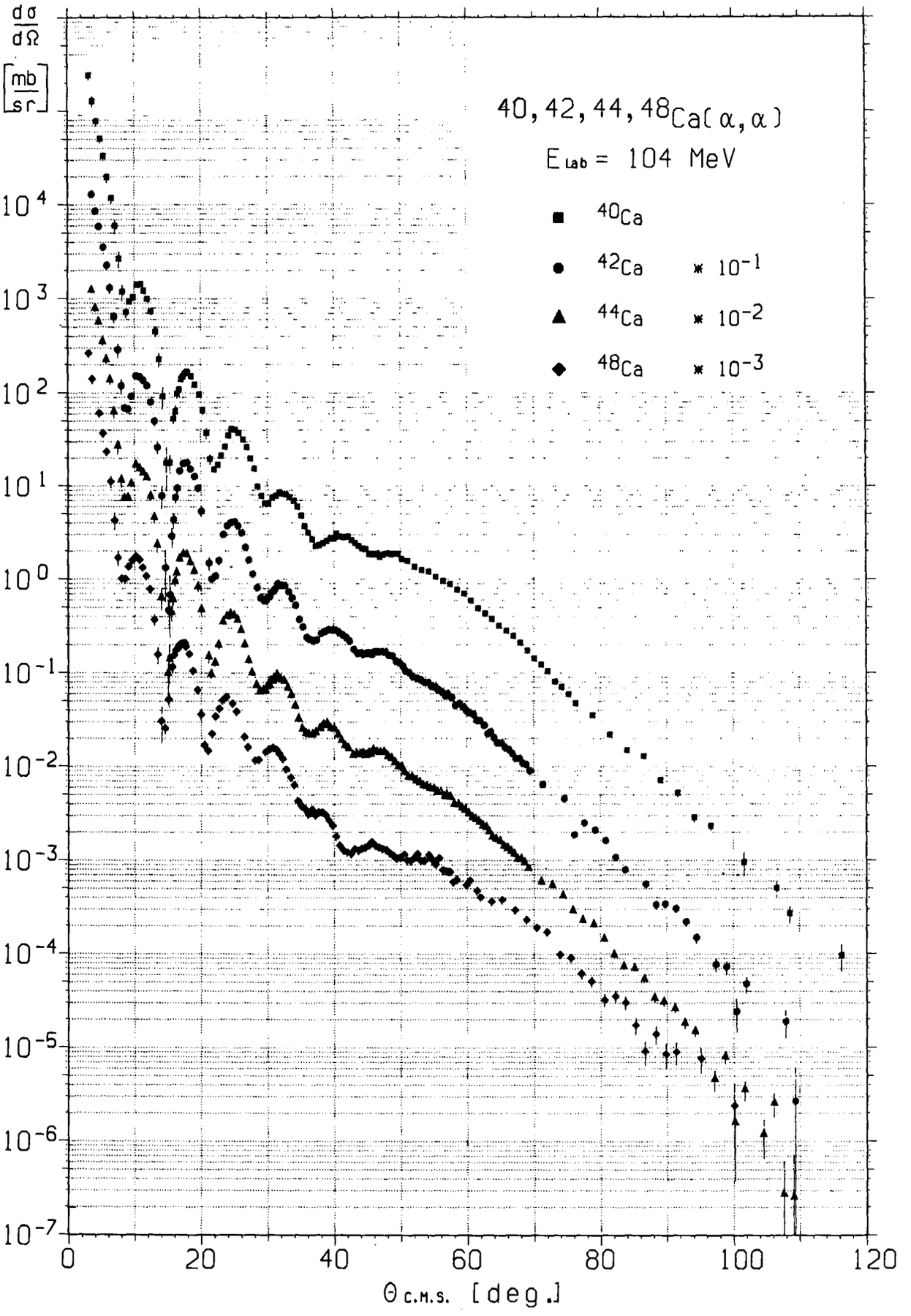

Fig. 1 Experimental differential cross sections for the scattering of 104 MeV α particles from $^{40,42,44,48}Ca$.

3. ANALYSIS

3.1 Conventional Optical Potentials

As a first step the analysis started with the conventional Saxon-Woods (SW) parametrization of the optical potential. Indepedent parameter sets were used for the real and imaginary parts, and the Coloumb potential was derived from realistic charge distributions of the projectile and target nuclei as determined from electron scattering experiments[6]. The parameter values and some integral quantities of the resulting potentials are quoted in Table 1a. The best values of χ^2/F, χ^2 per degree of freedom, were significantly larger than 1 indicating that the SW optical potential was inadequate for describing the observed differential cross sections. This phenomenon had been noticed previously[7] with high-accuracy scattering data extending to large angles, and it was one of the motivations for the search for alternative forms of the optical potential[7,2]. It has become popular[7] recently to use the square of the SW function (SW^2) for the real potential. The difference between this form and the conventional SW form lies in the coupling between the surface region and the interior of the nucleus. We found indeed that the SW^2 form lead to better χ^2/F in fitting the measured data, as indicated in Table 1b. It is also obvious that the characteristic parameters depth, half-way radius and skin thickness as well as the integral quantities obtained for each particular isotope are different for the alternatively used potential forms SW or SW^2, respectively. The differences between the integral quantities of the different isotopes, however, are nearly indepedent from the choice of the functional form of the potential.

In a further step we introduced the SW^2 form also in the imaginary part of the optical potential. Thereby, the χ^2-values were only slightly reduced. Even if a surface absorption with three additional free parameters was included no further significant improvement of the theoretical description was achieved (see table 1c, d). In the latter case the six parameters of the imaginary potential were <u>not</u> unambigously determined in contrast to the cases without surface absorption. (The measured data could not at all be described when taking solely the surface term without volume absorption). The parameters and particularly the volume integral per nucleon pair of the <u>real</u> potential significantly changed when using differ-

Table 1a: Parameters of Saxon-Woods potentials

	Real Potential					Imaginary Potential					
A	V_o [MeV]	r_v [fm]	a_v [fm]	$-J_v/4A$ [MeV fm^3]	$\langle r_v^2 \rangle^{1/2}$ fm	W_o [MeV]	r_w [fm]	a_w [fm]	$-J_w/4A$ [MeV fm^3]	$\langle r_w^2 \rangle^{1/2}$ fm	χ^2/F
40	126.0	1.221	0.829	333.9	4.466	18.8	1.666	0.588	100.6	4.925	6.5
42	117.0	1.258	0.803	325.1	4.513	20.1	1.665	0.580	106.8	4.975	7.1
44	116.7	1.260	0.794	321.6	4.536	21.6	1.641	0.593	110.3	5.000	4.4
48	130.8	1.216	0.823	330.5	4.589	18.4	1.657	0.558	95.1	5.105	3.4
	Table 1b: Parameters of real SW^2-potential and imaginary SW-potential										
40	152.6	1.404	1.253	317.9	4.315	20.3	1.603	0.678	100.9	4.938	3.7
42	138.1	1.446	1.196	312.1	4.372	22.3	1.603	0.653	109.2	4.952	4.1
44	139.4	1.438	1.189	310.0	4.394	24.0	1.578	0.665	112.6	4.973	3.6
48	162.1	1.378	1.274	318.6	4.458	18.9	1.633	0.603	95.0	5.114	3.3
	Table 1c: Parameters of SW^2-potentials (real and imaginary)										
40	167.9	1.341	1.342	309.4	4.315	22.0	1.789	1.043	96.0	4.892	3.6
42	152.9	1.382	1.287	304.5	4.360	23.1	1.791	0.988	101.9	4.916	3.2
44	152.6	1.381	1.272	302.4	4.381	25.8	1.753	1.036	106.0	4.931	3.1
48	179.4	1.312	1.368	308.6	4.450	20.2	1.791	0.921	90.6	5.057	3.1

Table 1d: Parameters of SW^2-potentials (real and imaginary) plus surface absorptions W_s
(Imaginary potentials W_o and W_s are not unambignously determined)

	Real Potential					Imaginary Potential								
						Volume			Surface					
A	V_o [MeV]	r_v [fm]	a_v [fm]	$-J_v/4A$ [MeV fm^3]	$\langle r_v^2 \rangle^{1/2}$ [fm]	W_o [MeV]	r_w [fm]	a_w [fm]	W_s [MeV]	r_s [fm]	a_s [fm]	$-J_w/4A$ [MeV fm^3]	$\langle r_w^2 \rangle^{1/2}$ [fm]	$\frac{\chi^2}{F}$
40	130.2	1.511	1.118	335.8	4.366	23.1	1.34	1.87	12.8	1.515	0.766	111.8	5.065	2.9
42	135.6	1.460	1.169	315.5	4.369	12.3	1.35	1.65	15.5.	1.412	1.06	109.6	4.988	3.0
44	148.7	1.395	1.246	303.3	4.376	11.8	1.831	0.975	10.8	1.235	1.25	106.4	4.954	2.7
48	127.9	1.519	1.060	337.1	4.524	12.0	1.677	1.393	14.7	1.506	0.704	106.9	5.259	2.6

ent forms for the imaginary potential (compare tables 1b, c, d). This indicates a non-negligible coupling between the real and imaginary potential when using these simple functional forms.

As an example, the real and imaginary potentials of ^{40}Ca and ^{44}Ca are displayed in fig. 2 for the cases a, b, and d. The differences originating from the chosen functional form are of the same order of magnitude for both nuclei but the qualitative behaviour of the different models are different for ^{40}Ca and ^{44}Ca.

Besides the potentials itself it is useful to compare their integral moments which are defined as follows

$$M_K(V) = \langle r^K \rangle^{1/K} = \left[\frac{\int_0^\infty V(r) r^{K+2} dr}{\int_0^\infty V(r)\, r^2\, dr} \right]^{1/K} \qquad \text{for } K \neq 0$$

$$M_o = \exp \left[\frac{\int_0^\infty \ln r\, V(r)\, r^2\, dr}{\int_0^\infty V(r)\, r^2\, dr} \right] \qquad \text{for } K = 0 \qquad (1)$$

(The second moment M_2 is just the rms radius!)
The moments are plotted in fig. 3 for $K = -2$ up to $K=6$ for the real and imaginary potentials of the procedures a), b) and d) (compare table 1)

For the real potentials one observes strong deviations between the different approaches in particular for the higher moments ($K \gtrsim 2$). The moments of the imaginary potentials agree rather well at least for $^{42,44}Ca$. In general, a great similarity between the behaviour of the potentials of the spherical nuclei $^{40,48}Ca$ on the one hand and between the possibly deformed nuclei $^{42,44}Ca$ on the other hand, can be observed (see also Appendix B).

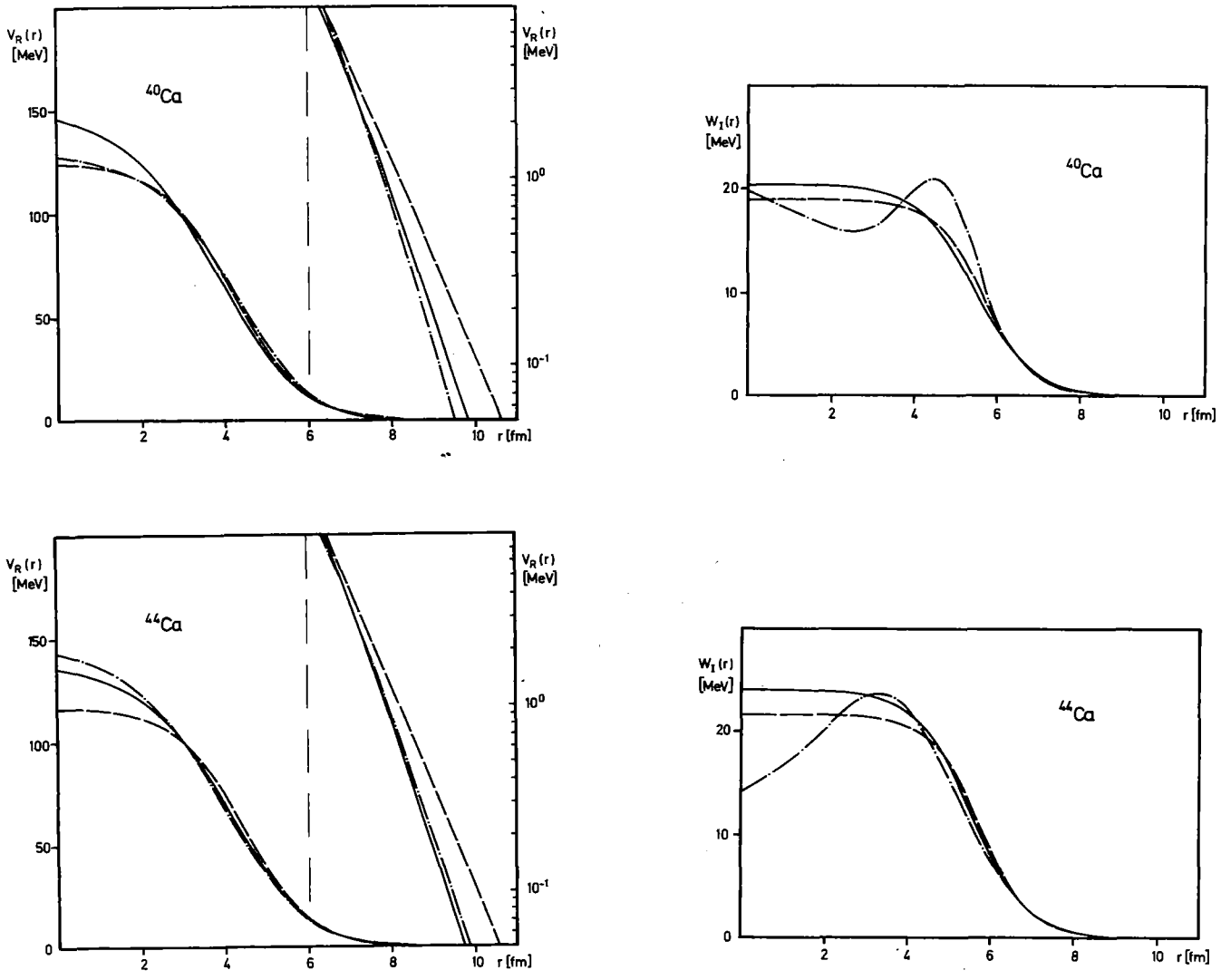

Fig. 2 Real and imaginary potentials for $^{40}Ca(\alpha,\alpha)$ and $^{44}Ca(\alpha,\alpha)$ using different approaches. Dashed lines: $SW_R + SW_I$; solid lines: $SW_R^2 + SW_I$; dashed-dotted lines: $SW_R^2 + SW_I^2$

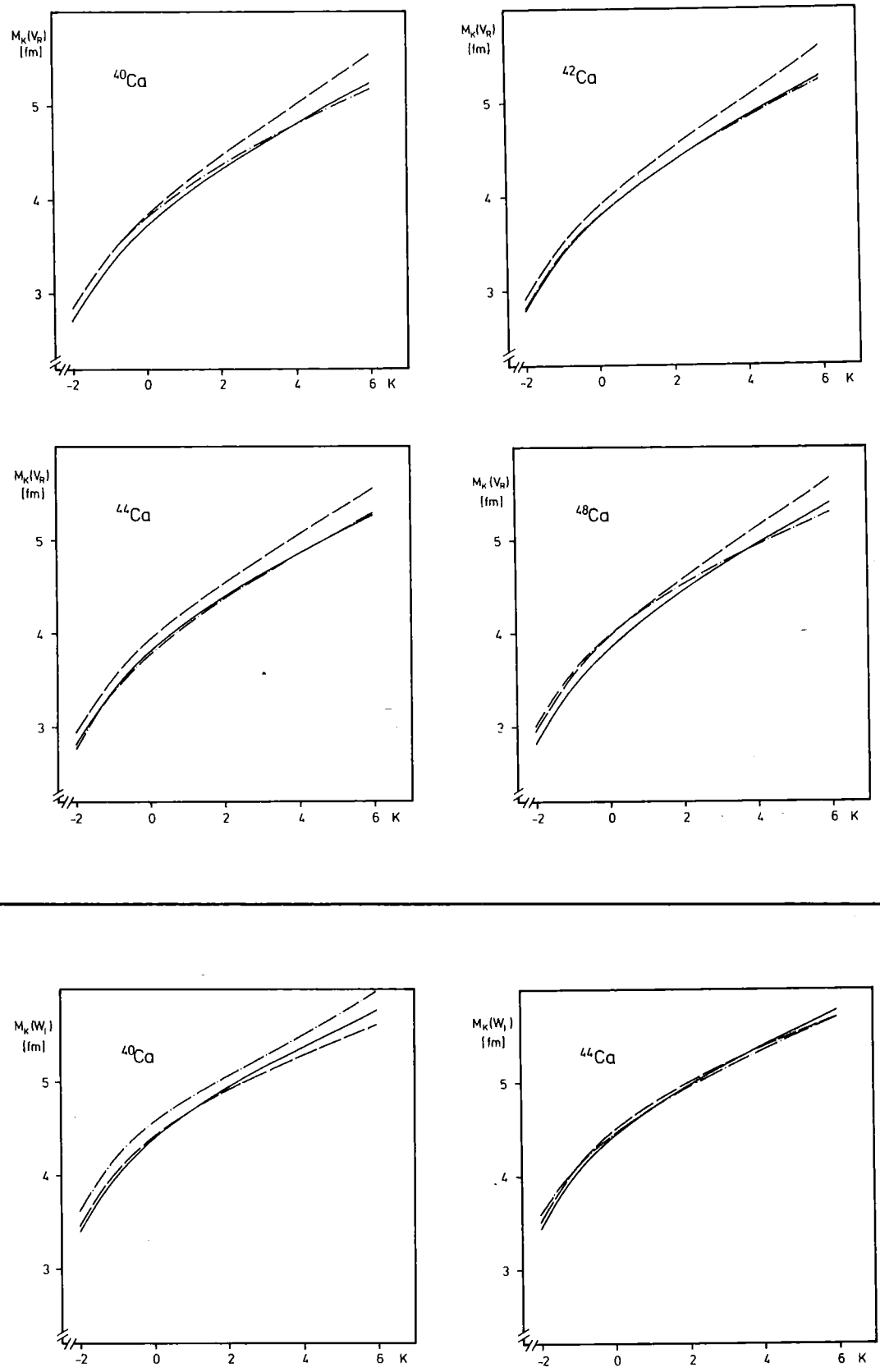

Fig. 3 Integral moments M_K (eq. 1) of the real and imaginary potentials using different functional forms (compare fig. 2)

3.1 Fourier - Bessel - Potentials

The SW^2 form is just another parametrization of the shape of the optical potential and, like the SW form, it cannot be considered suitable for studies of a series of isotopes since the choice of a particular simple functional form for the potential may introduce some bias into the results, as indicated above. In order to reduce such effects the real part of the optical potential U was written[2] more flexibly as

$$\text{Re } U(r) = -V_o(r) - \sum_{n=1}^{N} b_n \, j_o \left(\frac{n\pi r}{R_c}\right) \qquad (2)$$

where $V_o(r)$ was either a SW or a SW^2 best fit potential and where the series of spherical Bessel functions was included only for $r \leq R_c$, with a suitably chosen cut-off radius R_c (usually 10-13 fm). The N coefficients b_n ($N \sim 10\text{-}13$) were obtained by adjustment to the experimental data. The imaginary potential was of the SW or SW^2 form and was adjusted simultaneously with the FB series. The term $V_o(r)$ served only as the initial potential for the FB fit. By using the FB-analysis two main goals are achieved[2]: (i) Sufficient flexibility is introduced into the potential form thus allowing a better description of the differential cross sections, whereby the constraints due to the choise of particular functional forms of $V_o(r)$ are avoided. (ii) Realistic estimates are obtained for the uncertainties of various quantities such as the real potential itself, the volume integral, and the rms radius. Uncertainties claimed for results of conventional analyses are often underestimated[3] because the potential region to which the experimental data are not sensitive is simulated to be known via the extrapolation of a particular functional form.

Figure 4 displays examples of the fits obtained for the ^{40}Ca data. The improvement in the fits when going from SW to SW^2 and to the FB option is clearly observed. It should be emphasized that the shape of the imaginary potential was of the SW or SW^2 form . That could have some residual effect on the real potential. However, this effect is found practically negligible (see Appendix B). Fig. 5 shows FB fits to all four Ca isotopes and it demonstrates the excellent description of the experimental cross sections

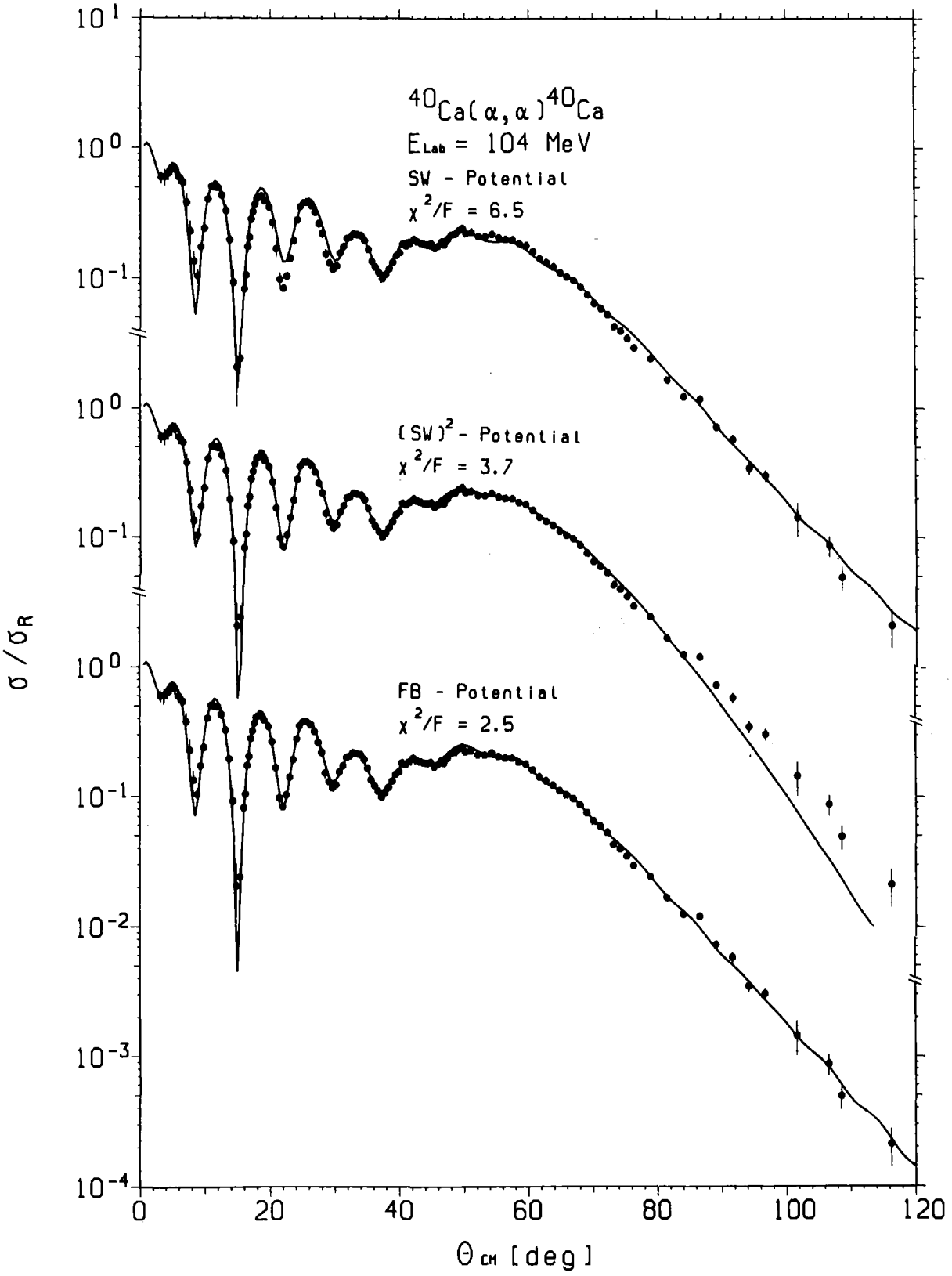

Fig. 4 Results of optical model analysis of 104 MeV α particle scattering from ^{40}Ca using different parametrization.

obtained with FB potentials. Table 2 summarizes the results for integral quantities of interest. These were obtained from averaging various FB fit potentials with SW^2 form for the initial real potential V_o and a SW form for the imaginary potential. The determination of the errors is described in Appendix A.[11]

Table 2. Integral quantities of the FB potentials

Target	χ^2/F	$-J_V/4A$ (MeV fm^3)	$\langle r_v^2 \rangle^{1/2}$ (fm)	$-J_w/4A$ (MeV fm^3)	$\langle r_w^2 \rangle^{1/2}$ (fm)
^{40}Ca	2.0	327 ± 3	4.37 ± 0.06	103	4.94
^{42}Ca	2.5	317 ± 3	4.38 ± 0.06	110	4.93
^{44}Ca	2.7	314 ± 3	4.41 ± 0.07	112	4.96
^{48}Ca	2.3	319 ± 5	4.49 ± 0.09	96	5.09

The final FB-potentials and various integral moments (eq.1) and their corresponding error bands are displayed in fig. 6 and fig. 7, respectively.

In order to demonstrate the dependence of the obtained error band on the angular data range included into the analysis the relative errors of the ^{48}Ca potentials are shown in fig. 8 for one particular set of R_c = 12 fm and N = 10.

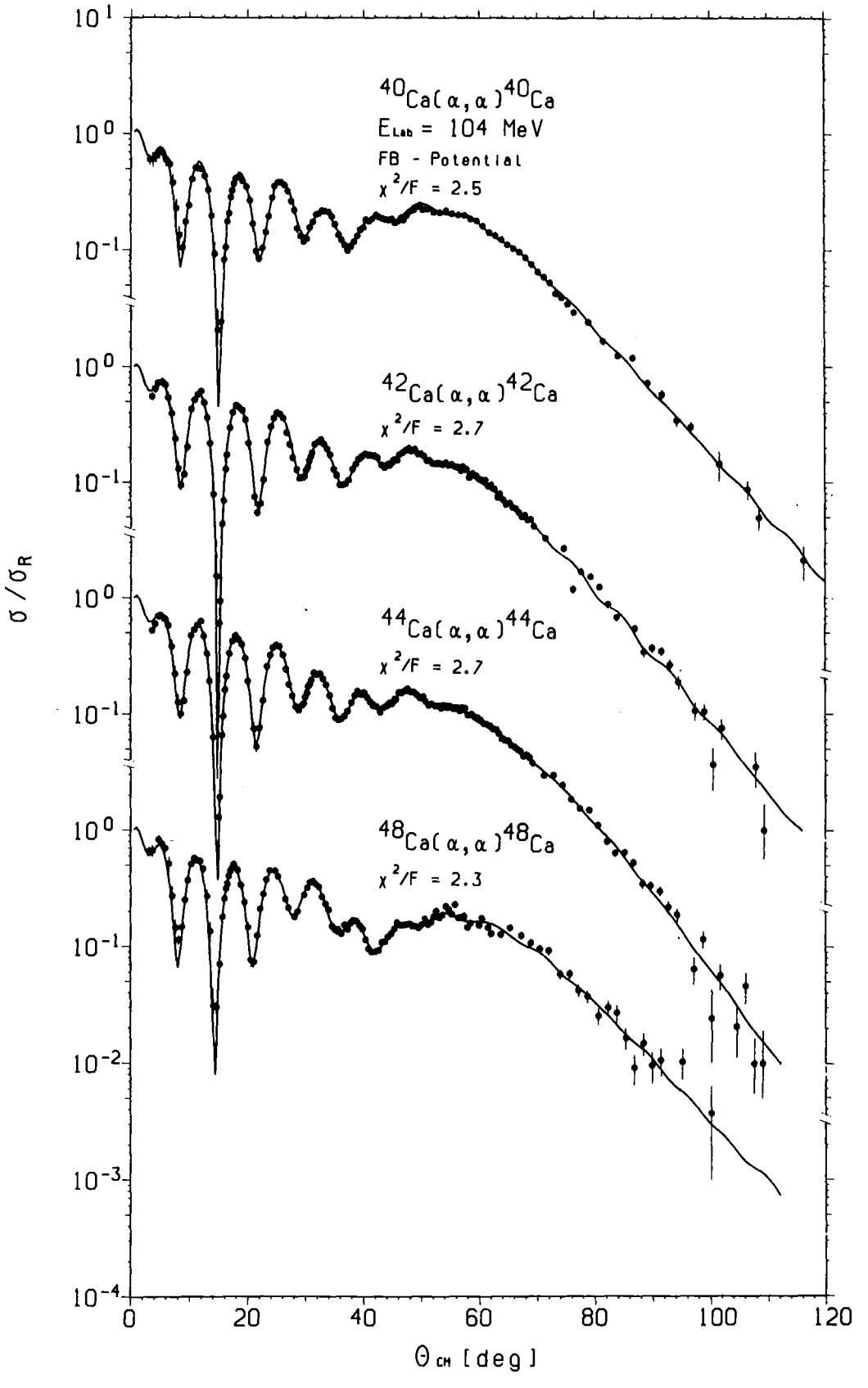

Fig. 5 Results of the Fourier-Bessel Method: Experimental and best-fit calculated differential cross sections.

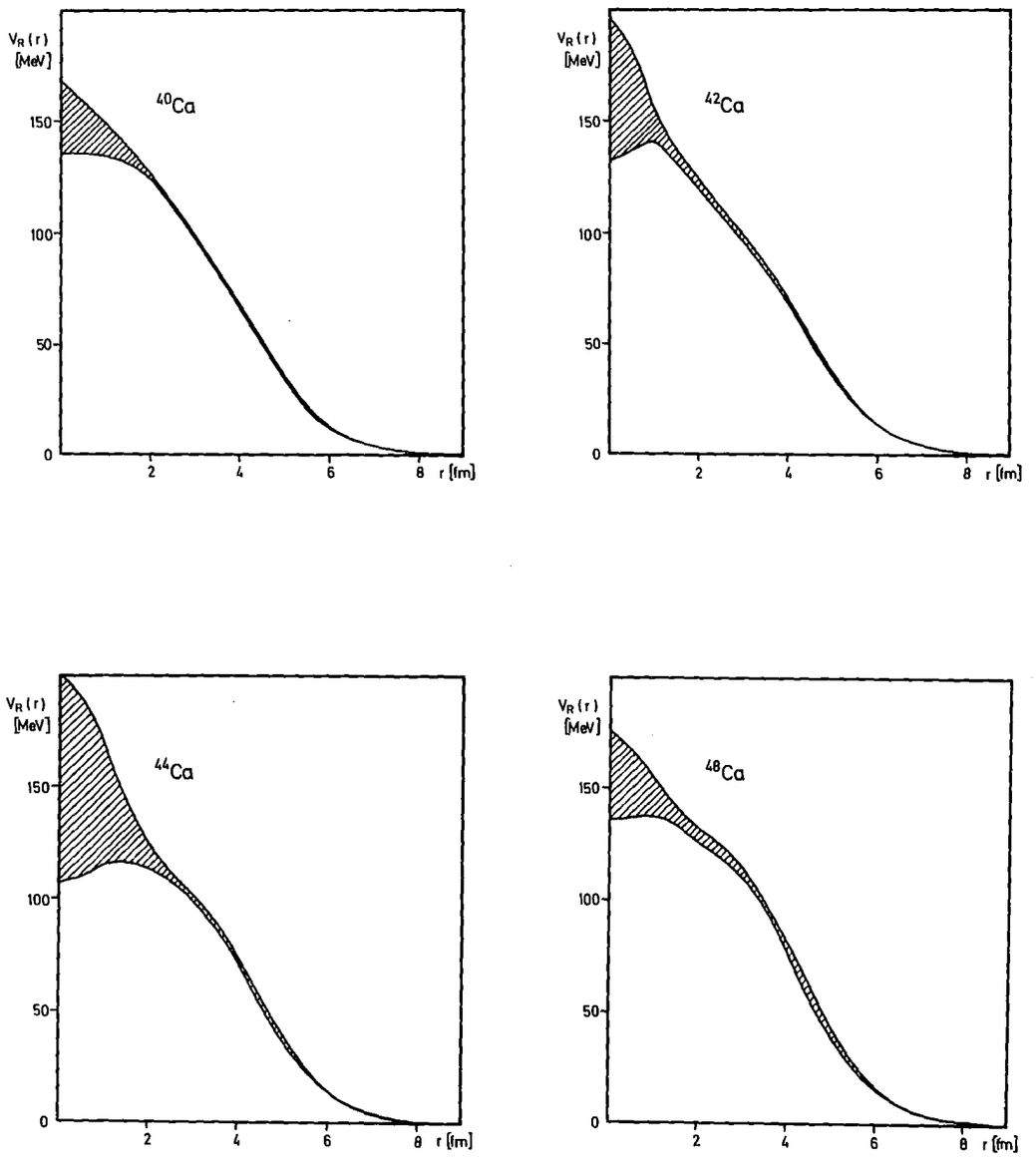

Fig. 6 Real optical potentials for elastic 104 MeV α-particle scattering from $^{40,42,44,48}Ca$ determined by the FB method. The hatched areas are the error bands.

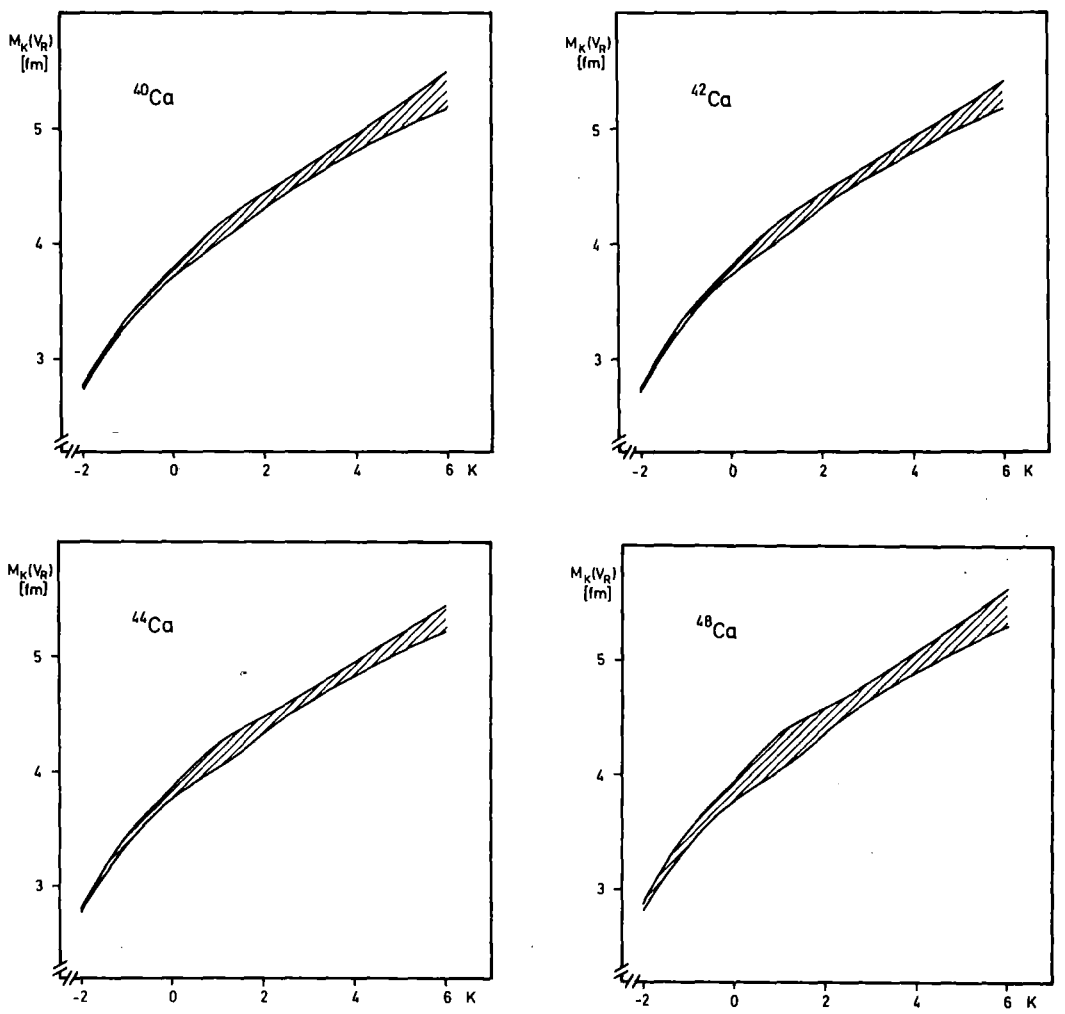

Fig. 7 Various integral moments (see eq. 1) of the real optical potentials including the corresponding error bands (hatched areas)

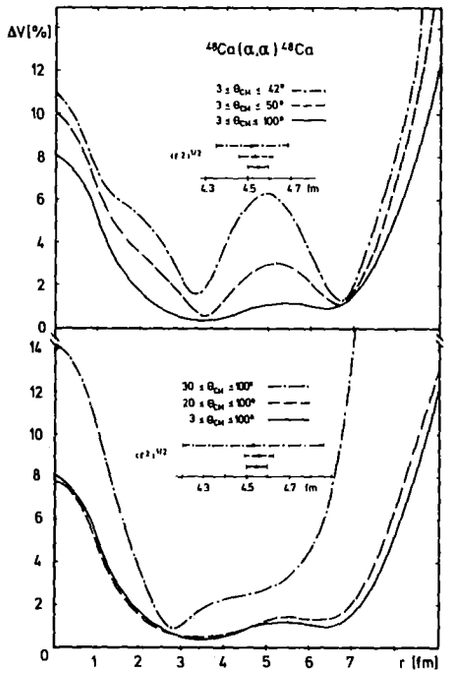

Fig. 8 Relative errors of the optical potential for ^{48}Ca. The different curves correspond to different restricted ranges of the data points used for the analyses.

It is obvious that the optical potential is best determined in the radial region between 2 and 7 fm, respectively, where the errors are smaller than 2 %.

When excluding the data points beyond the nuclear rainbow angle one still obtains small errors at r ∿ 7 fm which is the strong absorption radius as indicated by the dashed lines in the upper part of Fig. 8. The errors in the innermore part of the potential especially at the slope, however, are drastically increased and consequently also the errors of the rms-radii (see inset in Fig. 8). On the other hand, when excluding the very forward angle data from the analyses the error band at larger radii remarkably increases (Fig. 8, lower part) underlining the importance

of the forward angle data for a precise determination of the outer tail of the potential. The error band is also increased at larger radii ($r \gtrsim 3$ fm) by a factor of about two when taking larger angular steps of the data points (1.5^{o} instead of 0.5^{o}).

A possibly remaining model dependence of the optical potential when using the FB-method is discussed in Appendices A and B.

4. DISCUSSION

Although the FB method proved to be quite appropriate for the analysis of precisely measured elastic scattering cross sections extending to large scattering angles the failure to reach χ^2/F values closer to one indicates some residual deficiency. As already mentioned one possibility is, obviously, that the imaginary potential is not sufficiently flexible. But there are indications*) that an additional flexibility of the imaginary potential (e.g. by introducing a surface term with three additional parameters) do not significantly improve the χ^2/F values. The results may also be affected by the coupling of the elastic scattering to inelastic channels. Explicitly including such effects by a coupled channel analysis could possibly further reduce the values of χ^2/F. It should be remembered, however, that the description of the scattering cross sections on the basis of a local potentials is, in itself, an approximation. It is not unlikely that values of $\chi^2/F \sim 1$ cannot be achieved at all for high precision data within such an approach.

The results of the present work provide information on differences between the α particle-nucleus optical potentials for the calcium isotopes. In Fig. 9 the differences between the real parts normalized to their respective volume integral are shown in analogy with similar curves usually presented for the charge distributions.

The approximate equality of the volume integral per nucleon pair of the real potential ($J_V/4A$ in Table 2) suggests a folding model[8] interpretation. A folding model with a density independent effective interaction leads to a constant value of $J_V/4A$. This condition is not met exactly by

---

*) See Appendix B

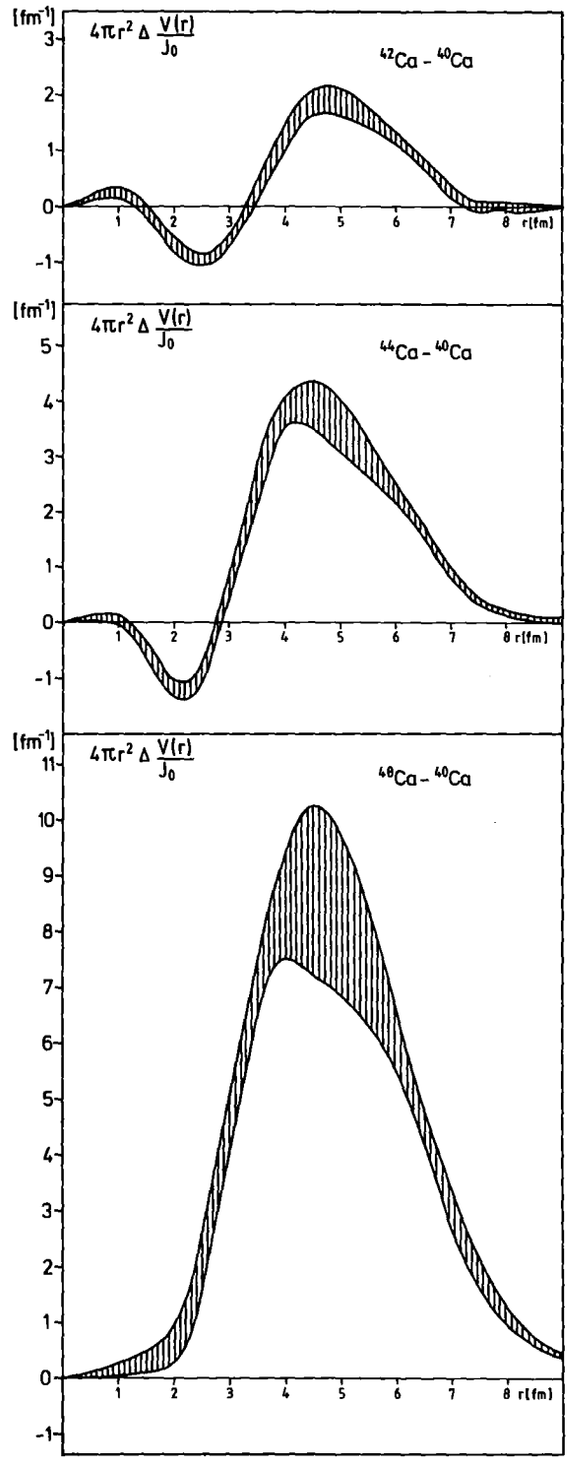

Fig. 9 Differences between real potentials obtained from the Fourier-Bessel analysis of 104 MeV α particle scattering.

the results of the FB fits. The small deviations may indicate some density dependence of the microscopic interaction, which also implies that the additivity of the mean square radii of the α particle-nucleon effective interaction $\langle r^2_{\alpha N} \rangle$ and of the nuclear density distribution $\langle r^2_m \rangle$

$$\langle r^2_{\alpha N} \rangle + \langle r^2_m \rangle = \langle r^2_{pot} \rangle \qquad (3)$$

(which holds in a density independent folding model) has to be considered only as an approximation.

The study of nuclear density distributions and nuclear sizes is the topic of another paper[4] where the above questions will be discussed in detail. In particular it will be shown that the additivity of the mean square radii remains quite reliable. Anticipating the justification[4,10] of eq. 3, and introducing the information about the charge distribution[9] the difference of the rms radii of the real potentials reflects a small neutron skin of ^{48}Ca.

We wish to thank Professor Dr. G. Schatz and Professor Dr. P. Brix for their encouragement and continuous interest in this project. Valuable comments of Professor Dr. K: Grotowski are gratefully acknowledged. The cyclotron staff providing the α particle beam with excellent quality has contributed very much to the success of the experiments.
We wish to thank Mrs. K. Feisst for help for the calculations.

[1] D.A. Goldberg and S.M. Smith; Phys. Rev. Lett. 29, 500 (1972).

[2] E. Friedman and C.J. Batty, Phys. Rev. C 17, 34 (1978).

[3] E. Friedman, H.J. Gils, H. Rebel and Z. Majka, Phys. Rev. Lett. 41, 1220 (1978).

[4] H.J. Gils, E. Friedman, Z. Majka and H. Rebel, KfK-Report 2839.

[5] H. Rebel, G.W. Schweimer, G. Schatz, J. Specht, R. Löhken, G. Hauser, D. Habs, and H. Klewe-Nebenius, Nucl. Phys. A 182, 145 (1972).

[6] C.W. de Jager, H. de Vries, C. de Vries: Atomic Data and Nuclear Data Tables 14, 479 (1974).

[7] A. Budzanowski, K. Grotowski, M. Grzywacz and A. Strzalkowski, Progress Report, Institute for Nuclear Physics, Cracow, 1972 (unpublished) D.A. Goldberg, Phys. Lett. 55B, 59 (1975)

[8] A.M. Bernstein, Advances in Nucl. Phys., ed. by M. Baranger and E. Vogt (Plenum Press, New York, 1969).
D.F. Jackson and V.K. Kembhavi, Phys. Rev. 178, 1626 (1969).

[9] H.D. Wohlfahrt (Los Alamos), J. Friedrich (Mainz) private communication. Proc. International Discussion Meeting "What do we Know about the Radial Shape of Nuclei in the Ca-Region?", Karlsruhe, May 2-4. 1979, Report KfK 2830.

[10] Z. Majka, H.J. Gils, H. Rebel, in Proc. International Discussion Meeting "What do we Know about the Radial Shape of Nuclei in Ca-Region?", Karlsruhe, May 2-4, 1979, Report KfK 2830 - Acta Physica Polonica (in press)

[11] H.J. Gils and E. Friedman; in preparation.

Appendix A

Determination of errors of the Fourier-Bessel Potentials and their various integral quantities

A - 1 Errors of a single fit

The determination of the errors of the potential itself, the root-mean-square radius and the volume integral from any particular fit (one set of cut-off raddius R_c and number of parameters N) was described in detail in the paper of Friedman and Batty[2]. It should be noticed that in eq. 5 of that paper a factor of 2 was missing on the right-hand side. Correctly it must read

$$\langle \Delta b_m \, \Delta b_n \rangle_{av} = 2 \cdot (M^{-1})_{mn} \cdot f_{min} \overset{!}{=} C_{mn}$$

The equations for calculating the errors of higher and lower moments (see eq. 1 of the main part of this paper) than those given in ref. 2 are compiled below with the following notations

$$R'_K = \frac{4 R_c^{K+3}}{\pi}$$

$$C'_{mn} = \frac{(-1)^{m+n}}{m^2 n^2} \quad C_{mn} \qquad \text{(A - 1)}$$

$$\Delta(\langle r^K J \rangle) = R'_K \left[\sum_{n,m=1}^{N} C'_{mn} \cdot F_m^K \cdot F_n^K \right]^{1/2} \qquad \text{(A - 2)}$$

The terms F_n^K are defined by

$$\frac{(-1)^{n+1}}{n^2} \cdot \frac{4 R_c^{K+3}}{\pi} F_n^K = 4\pi \int_0^{R_c} r^{K+2} \, j_o\left(\frac{n\pi r}{R_c}\right) dr \qquad \text{(A - 3)}$$

and by a straightforward integration it can be shown that they satisfy the following relationship

$$F_n^K = 1 - \frac{K(K+1)}{\pi^2 n^2} F_n^{K-2} \, . \qquad \text{(A - 4)}$$

With the following results

$$F_n^{-1} = 1 + (-1)^{n+1} \qquad (A - 5a)$$

$$F_n^{o} = 1 \qquad (A - 5b)$$

it is easy to calculate F_n^K for $K \geq 1$. For $K = -2$ the following result is obtained

$$F_n^{-2} = \frac{(-1)^{n+1}}{n} \pi Si(n\pi) \qquad (A - 5c)$$

where $Si(n\pi)$ is the sine integral, with $Si(\infty) = \frac{\pi}{2}$. Setting K=0 in eq. (A-2) the error of the volume integral J is obtained. The relative error of the K-th moment, M_K ($K \neq 0$) is obtained from

$$\frac{\Delta M_K}{M_K} = \frac{1}{|K|} \left[\frac{\Delta \langle r^K J \rangle}{\langle r^K J \rangle} + \frac{\Delta J}{J} \right] \qquad (A - 6)$$

where J and $\langle r^K J \rangle$ are evaluated numerically by integrating to sufficiently large radius ($\approx$ 15 fm). (For $r > Rc$ only $V_o(r)$ is retained in the integration. The effects on the errors are discussed below.)

It is also interesting to define a zeroth radial moment not by setting K=0 in eq. (A-2) but by doing it as in eq. (1) of the paper, thus

$$M_o = \lim_{K \to 0} \left[\left\{ \frac{1}{J} \int_o^\infty 4\pi r^{K+2} V(r) dr \right\}^{1/K} \right]. \qquad (A - 7)$$

taking logarithms,

$$\ln M_o = \lim_{K \to 0} \left[\frac{1}{K} \{ \ln \int 4\pi r^{K+2} V(r) dr - \ln J \} \right] \qquad (A - 8)$$

which yields "0/0". Differentiating with respect to K and then letting $K \to 0$, we find

$$\ln M_o = \frac{1}{J} \int_o^\infty 4\pi r^2 (\ln r) V(r) dr \qquad (A - 9)$$

which leads to the second part of eq. (1) in the present paper. The error of the M_o moment (using the FB fits) is given by

$$\frac{\Delta M_o}{M_o} = \frac{\Delta J}{J} + \frac{\Delta\langle \ln r \cdot J\rangle}{\langle \ln r \cdot J\rangle} \qquad (A - 10)$$

with $\Delta\langle \ln r \cdot J\rangle$ given by eq. (A-2) with

$$F_n^{\ln} = \ln R_c + \frac{(-1)^n}{n\pi} Si(n\pi) \qquad (A - 11)$$

A - 2 Errors of the averages of several fits

The results and the errors of a single fit to the data may depend on the chosen cut-off radius R_c and on the number of FB-terms N. The influence of this choice was studied by performing 49 different fits with cut-off radii varying between 8 and 14 fm in steps of 1 fm and the number of FB-parameters N being between 8 and 14. A second aim of this study was to remove any remaining model dependence of the results of a single fit by determining - in an adequate way - averaged results and errors from the various individual calculations. The calculations were performed for each of the $^{40,42,44,48}Ca$ isotopes. Since the results obtained were very similar for all nuclei the investigations will be discussed using the example of ^{40}Ca.

The range of the number of varied FB-terms N was restricted by the facts that for $N < 7$ the reproduction of the experimental cross sections was distinctly worse whereas for $N > 14$ convergence problems of the fitting procedure became serious. The chosen range of the parameter R_c will be shown to be reasonable in the following discussion.

In fig. A-1 the values of the real potential at r = 0 fm, 2 fm, 4 fm, 6 fm, 8 fm, and 10 fm, the rms-radii and the corresponding errors are plotted versus R_c and partly also versus N. This characterizes the maximum spread of the individual calculations and reveals possible dependence of the results on these parameters. Corresponding plots were also made for the other various integral quantities in order to study their behaviour. From the χ^2-values per degree of freedom ranging from 2.0 up to 3.2 it is obvious that the different calculations reproduce the experimental data nearly equally well, so that from this aspect a selection of individual results is not possible or required.

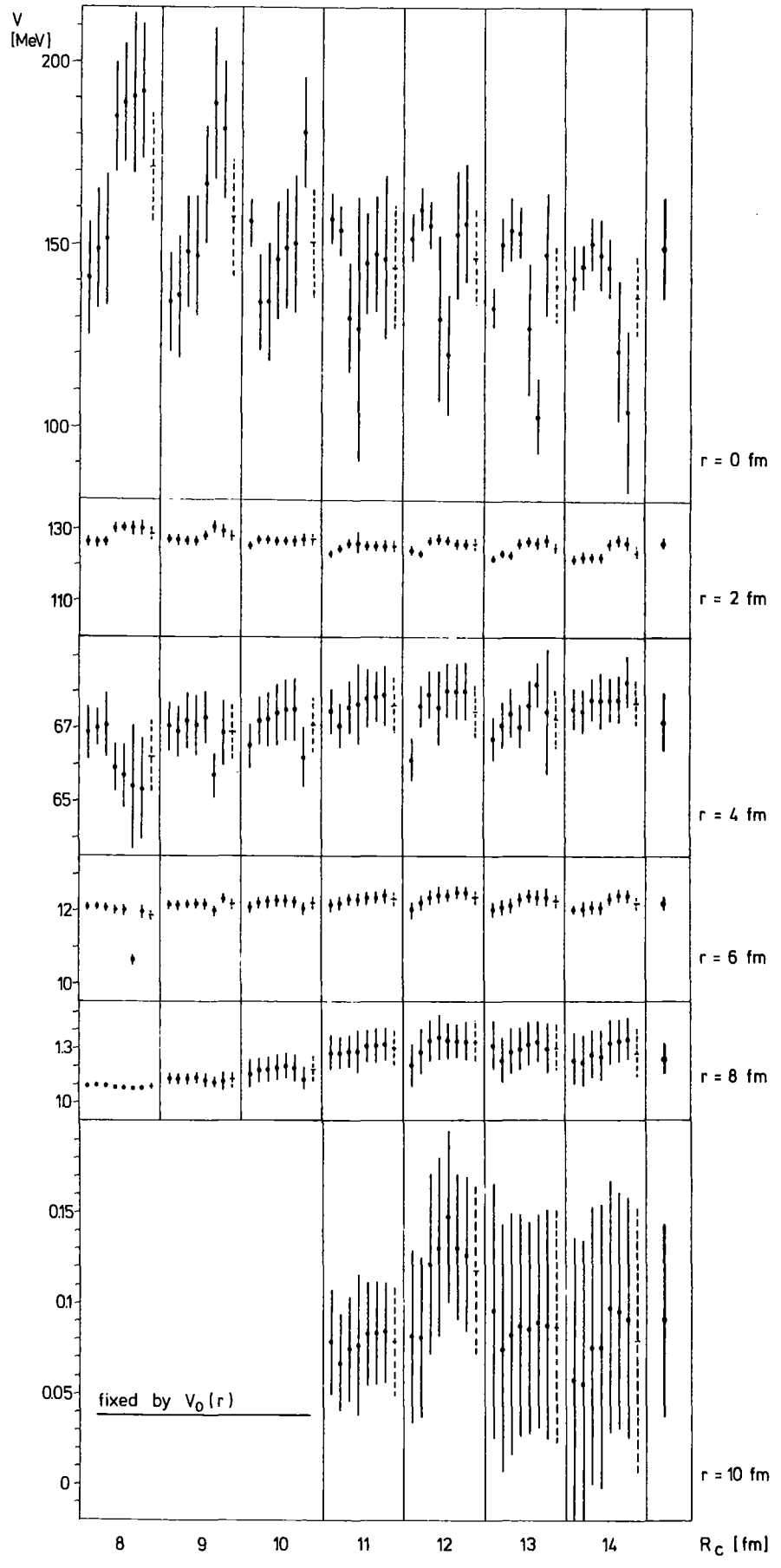

Fig.A-1a: Individual results and averages (dashed) of the potential values at different radii from various FB-fit calculations with different cut-off radii R_c and numbers of parameter N. The total averages are displayed in the right-hand column.

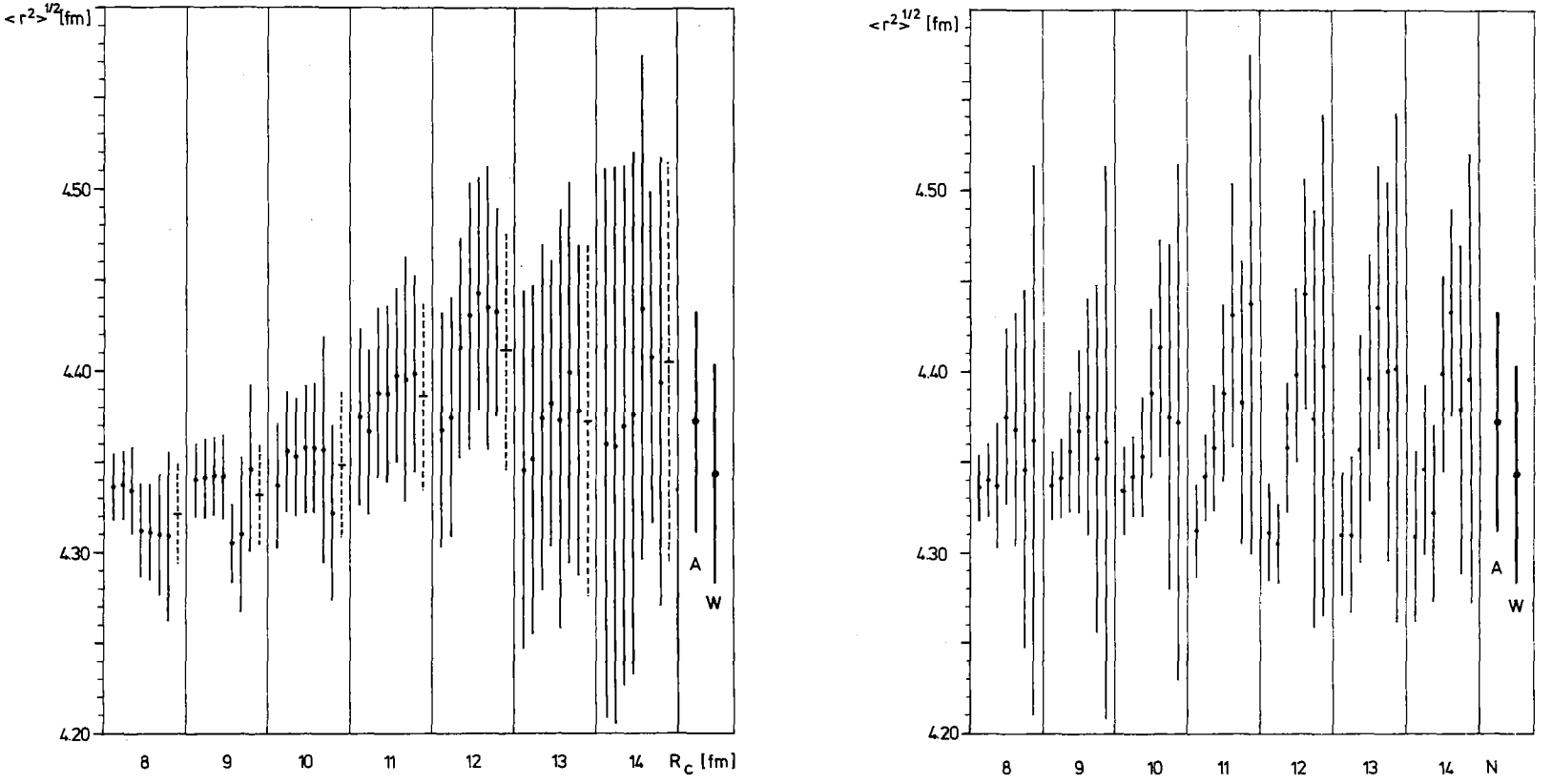

Fig.A-1b: Individual results and averages (dashed) of the rms-radii from various FB-fit calculations.

The results of the various individual calculations can be summarized as follows:

No systematic dependence on N was observed for

I (i) the potential for $r \gtrsim 2$ fm and $R_c \gtrsim 9$ fm
(ii) the volume-integral per nucleon pair, $-J_v/4A$
(iii) the K-th moments for K = -2 to +6
(iiii) the errors of all quantities evaluated

No systematic dependence on R_c was observed for

II (i) the potential between r = 2 fm and about 8 fm
(ii) the volume integral per nucleon pair
(iii) the moments smaller than K = 1
(iiii) the errors of the potential for $r < 7$ fm, of $J_v/4A$, and of the moments smaller than K = 1

Hence we oberve a dependence of the following quantities

III (i) the potential between r = o and r = 2 fm on R_c and N for $R_c \leq 9$ and $N \leq 9$
(ii) the potential for $r \gtrsim 7$ fm on R_c
(iii) the moments K = 1 to K = 6 on R_c
(iiii) the errors of the moments 1 to 6 on R_c

Fig. A-1 and compilations I-III show that most of the interesting quantities do not systematically depend on R_c and N. For these quantities it is at least reasonable to calculate the final value of the quantity by averaging the individual results thus cancelling out the accidental results of any individual calculation. Thereby there is no considerable difference between arithmetic or weighted mean value.

For the determination of the final errors of these quantities there is no standard procedure available, because the individual errors contain only the experimental errors (statistics, angular uncertainty) whereas the averaging procedure also considers model dependence. No estimates of these model dependent errors (if at all possible) are given by any well founded mathematical formalism (such as the statistical errors) nor their combination with the latter, when both contribute to the final error.

The most conservative error determination, of course, will be to quote

the maximum and minimum range of the individual error bars as the final error of each quantity. However, in view of the very small standard deviations

$$S = \sqrt{\frac{1}{n} \sum_{i=1}^{n} (\bar{X} - X_i)^2} \qquad (A - 12)$$

of the individual results X_i from the final average value $\bar{X}$ this seems us to be an overestimate. These standard deviations are for all quantities not listed under III distinctly smaller than the average of the individual errors and, of course, smaller than the total spread of the error bars. Hence, we quote the arithmetic mean value of the individual errors as the final errors of the quantities under consideration (not listed under III).

For the quantities, where we observe a dependence on the choice of R_c or N the dependence of the potential between r = o and r = 2 fm was only observed if <u>both</u> R_c and N were small (≤ 9). In these calculations the χ^2-values were systematically larger (around 3) than in the other calculations (average of χ^2-values about 2.5). This is certainly due to the fact, that with the restrictions $R_c \lesssim 9$ fm <u>and</u> $N < 9$ the FB-model is not flexible ('model independent') enough to give an optimal reproduction of the experiment. Therefore, we omitted these particular calculations in the further averaging procedure.

The only remaining dependence which should be discussed more in detail is the dependence on R_c of the potential values for $r \gtrsim 7$ fm, the dependence of the higher moments and in particular of the errors of these quantities. We start with the discussion of the increase of the errors with increasing R_c which seems to be the most serious problem. The increase of the errors of the higher moments is easy to understand since the error of the potential for radii larger than R_c but smaller than the integration limit (which was 14 fm in all calculations) by definition is set to zero. This deficiency - on the first glance - may lead to the conclusing that the cut-off radius has to be increased more and more, in order to get more realistic errors. However, there is a clear argument against a further increase of R_c. The radial region between r = 13 fm and r = 14 fm for example contributes to the value of the sixth moment only 0.03 % and to that of the second moment only 0.003 %. Hence further

increase in R_c is not justified. Therefore for the error determination of integral quantities only those individual calculations should be included where the free-fitted potential region $r < R_c$ really contributes to the quantity under consideration. As a criterion for the terminus "contributes" we chose the following: a further integration from R_c up to r = 14 fm should increase the quantity by at least 0.2 % (that is about $^1/10$ of the smallest individual error)*).

By this criterion one gets as maximum cut-off radius R_c to be considered for the error determination of the various integral quantities:

$$J_o/4A: \qquad R_c^{max} \approx 11 \text{ fm}$$

$$M_K: \; K = -2 \text{ to } +4 \qquad \approx 11 \text{ fm}$$

$$M_K: \; K = +5 \text{ to } +6 \qquad \approx 12 \text{ fm}$$

In order to avoid too strong an influence of accidental results of individual fits with the particular R_c-values quoted, we calculated the arithmetic average of the errors of all individual results with

$$R_c = R_c^{max} \pm 1 \text{ fm}$$

Thereby, one gets an error of the rms-radius of ^{40}Ca of

$$\Delta_1 = 0.06 \text{ fm}$$

This error determination seems to be rather conservative for the following reasons:

(i) The maximum spread $^1/2 \cdot (\langle r^2 \rangle_{max}^{1/2} - \langle r^2 \rangle_{min}^{1/2})$ of all individual results (R_c = 8 - 14 fm, N = 8 - 14) is only slightly larger, namely

$$\Delta_2 = 0.07 \text{ fm}$$

(ii) The standard deviation respecting all individual results is determined to be

$$\Delta_3 = S = 0.04 \text{ fm}$$

---

*) When increasing the critical value to 1 %, the errors of the moments K > 1 are <u>decreased</u> by about 50 %!

Similar relations between the characteristic quantities Δ_1, Δ_2 and Δ_3 hold also for the other integral quantities.

The average value $\bar{X}$ itself of each integral moment was determined from all calculations with 9 fm $\leq R_c \leq$ 13 fm. This somewhat wider region was used to reduce the influence of the starting potential V_o and of the integration limit R_{max}=14 fm. For comparison, we calculated also the weithted average (W) of the rms-radius (displayed in Fig. A-1) which agrees within the error bars with the arithmetic average (A) although the calculations with smaller R_c have a stronger weight on this average.

Concluding, it seems fair to say that accidental results dominated by a particular choice of R_c and N are satisfyingly cancelled out by the averaging procedure described above and that the quoted errors also include model dependent effects of the FB-method. The quoted errors, however, do not include those model effects which are not directly connected with the FB-method. The quoted errors, however, do not include those model effects which are not directly connected with the FB-method, as e.g. the chosen functional form of the imaginary potential *). This kind of model dependence is discussed in Appendix B.

---

*) The errors of the parameters of the imaginary potential enter the error determination of the FB method via the covariance matrix (eq. A - 1) which includes the correlations of the FB-parameters with the parameters of the imaginary part.

Appendix B

Remarks on the model dependence of the FB-optical potentials on $V_o(r)$ and on the form of the imaginary potentials

The most important model assumptions which are still involved in the FB-analyses are obviously the preselected forms of the "first guess" potential $V_o(r)$ (eq. 2) and of the imaginary potential W_I taking either SW or SW^2 parametrization. In order to study the influence of the chosen functional form of V_o and W_I on the final FB-potential we performed four different "sets" of FB-calculations which are characterized in table B-1:

Table B-1: FB-calculations using different parametrizations for $V_o(r)$ and $W_I(r)$

Set	V_o	Parameters of V_o from table	W_I
1	SW	1a	SW
2	SW^2	1b	SW
3	SW^2	1d	SW
4	SW^2	1d	SW^2 + surface

The calculations of set 1,2 and 4 were performed for $^{40,42,44,48}Ca$, set 3 only for ^{40}Ca.
The different starting potentials $V_o(r)$ are displayed in fig. 2 (main part of this paper) for ^{40}Ca. The first three sets mainly aim at investigating the influence of $V_o(r)$ (different $V_o(r)$ but same form of $W_I(r)$). Set 3 and 4 have the same real starting potential $V_o(r)$ but distinctly different imaginary potentials (see fig. 2). In the calculations of set 4 the surface term of the imaginary potential was not varied because of ambiguities. The parameters of the surface term were taken from table 1d. For each set 36 FB-fit calculations were performed and averaged as explained in Appendix A-2.

R_c = 9-14, N = 9-14

Although the starting potentials were quite different the final FB-potentials excellently agreed for $r \lesssim 8$ fm as demonstrated in fig.B-1 for the extreme cases 1 and 2

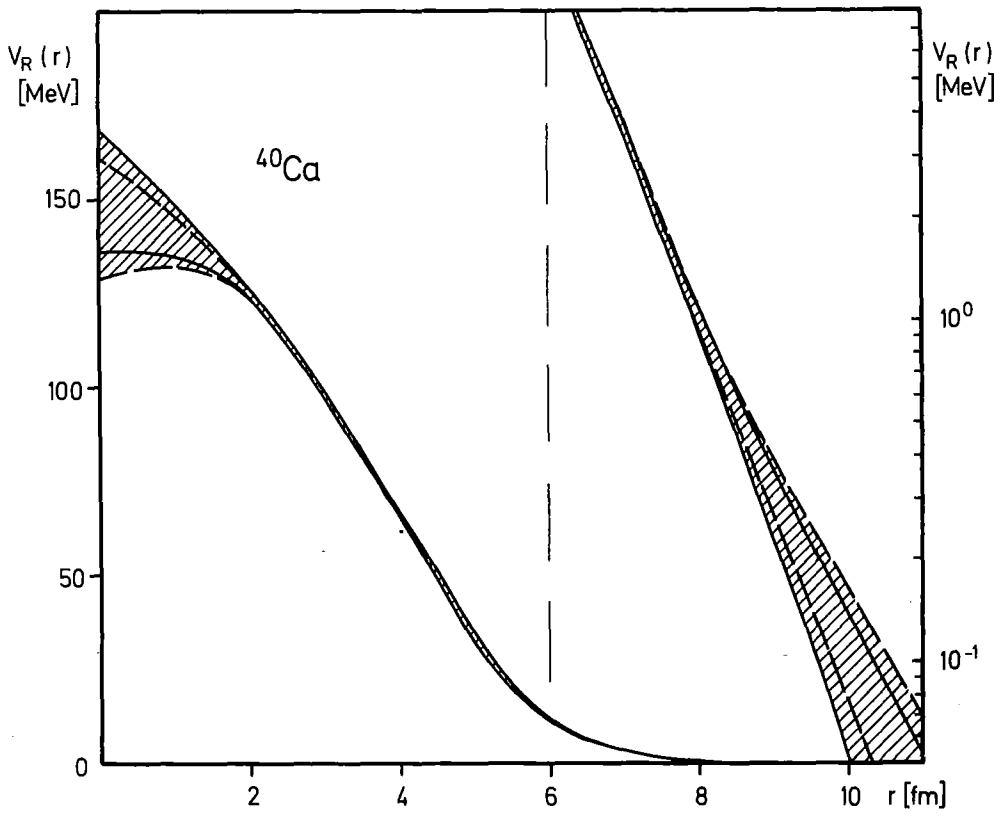

Fig. B-1 FB-potentials with error bands using different starting potentials $V_o(r)$. Dashed line: SW starting potential (Set 1); Solid line: SW^2 starting potential (Set 2).

At larger radii, however, the final potentials were mainly determined by the starting potential $V_o(r)$ since the scattering cross sections are not sensitive to this region (see fig. 7). Consequently the resulting rms-radii and in particular higher moments of the various procedures slightly differ from each other since the potential tail has a dominant weight on the higher moments.

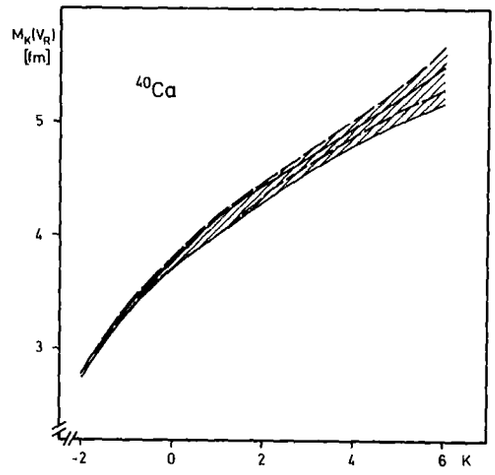

Fig. B-2 Integral moments M_k (see eq. 1) and corresponding error bands obtained by various FB-fit calculations with different starting potentials $V_o(r)$. Dashed line: SW (Set 1) Solid line: SW^2 (Set 2)

For the imaginary potentials of set 1 the starting values for the (varied) parameters were taken from table 1a; for sets 2 and 3 we used the values of table 1b. Although these potentials were rather different in *each individual FB-fit calculation of sets 1 to 3 the parameters of the imaginary potential converged to the same values* (within the range of the parameter-errors) which were very close to the values given in table 1b.

The influence of the form of the imaginary potential on the real FB-potential studied by set 3 and 4 is as small as the influence of $V_o(r)$. The real potentials itself overlap between r=0 and 10 fm similarly as shown in fig. B-1. The most obvious effect is the increase of the volume integral per nucleon pair - which agree for sets 1 to 3 within 2 MeV fm^3 - by about 7 MeV fm^3 *) and a less steep increase of the integral moments as demonstrated in fig. B-3.

---

*) Consider the error of ± 3 MeV fm^3 !

Thereby a complete agreement of the moments -1 to +1 is observed for all four sets of calculations.

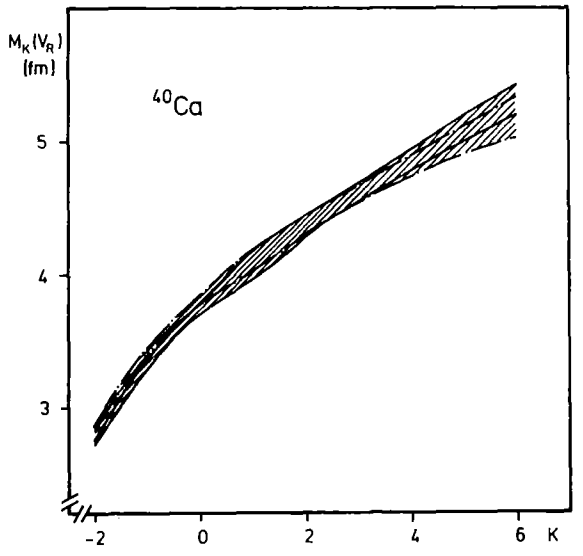

Fig. B-3 Integral moments M_K (see eq. 1) and corresponding errors band obtained for different forms of the imaginary potentials. Solid SW (set 3) Dashed dotted SW^2 (set 4)

From the various FB-calculations characterized in table B-1 and from figs. B-1 to B-3 we conclude that the results of some of the evaluated quantities slightly depend on the starting potential $V_o(r)$ and on the imaginary potential to an amount which is not in all cases fully inside the error bands provided by the FB-method.

However, for the most interesting quantities, namely the differences between the potentials of the Ca-isotopes and their integral moments any model dependence completely vanishes. Hence we regard the FB-method to be adequate at least to determine isotopic or isotonic differences of α-particle scattering potentials model independently.

Appendix C

Experimental Differential Cross Sections

SCATTERING OF 4-HE PARTICLES ON 40-CA

ELAB = 104.000 MEV Q = 0.0 MEV I = 0 +

ECM = 94.532 MEV K = 4.0567/FERMI ETA = 1.23581

LABORATORY DATA			RUTHERFORD	CM DATA		
THETA DEGREE	SIGMA MB/SR	DSIGMA %	SIGMA/SR	THETA DEGREE	SIGMA MB/SR	DSIGMA MB/SR
2.89	2.838E+05	11.3	6.015E-01	3.19	2.335E+05	2.627E+04
3.39	1.511E+05	15.2	6.061E-01	3.74	1.243E+05	1.893E+04
3.89	9.235E+04	11.7	6.423E-01	4.29	7.599E+04	8.889E+03
4.41	6.027E+04	10.4	6.904E-01	4.86	4.960E+04	5.133E+03
4.92	3.904E+04	11.4	6.931E-01	5.42	3.213E+04	3.677E+03
5.40	2.328E+04	12.5	6.008E-01	5.95	1.916E+04	2.392E+03
6.00	1.389E+04	12.8	5.463E-01	6.62	1.144E+04	1.466E+03
6.50	7.030E+03	18.4	3.806E-01	7.17	5.789E+03	1.068E+03
7.00	3.154E+03	21.5	2.296E-01	7.72	2.590E+03	5.592E+02
7.50	1.408E+03	20.4	1.350E-01	8.27	1.169E+03	2.366E+02
8.00	8.434E+02	13.3	1.047E-01	8.82	6.949E+02	9.221E+01
8.50	1.103E+03	5.7	1.743E-01	9.37	9.088E+02	5.164E+01
9.00	1.218E+03	6.8	2.419E-01	9.92	1.004E+03	6.846E+01
9.50	1.654E+03	5.0	4.075E-01	10.47	1.364E+03	6.876E+01
10.00	1.688E+03	3.1	5.105E-01	11.02	1.393E+03	4.382E+01
10.39	1.430E+03	4.9	5.037E-01	11.45	1.180E+03	5.834E+01
10.89	1.174E+03	5.9	4.988E-01	12.00	9.687E+02	5.702E+01
11.39	8.556E+02	8.3	4.348E-01	12.55	7.063E+02	5.833E+01
12.00	5.266E+02	12.0	3.295E-01	13.22	4.349E+02	5.241E+01
12.50	2.682E+02	18.7	1.974E-01	13.77	2.216E+02	4.153E+01
13.00	1.081E+02	27.5	9.307E-02	14.32	8.937E+01	2.455E+01
13.50	2.086E+01	50.4	2.087E-02	14.87	1.725E+01	8.698E+00
14.00	2.106E+01	23.8	2.435E-02	15.42	1.742E+01	4.149E+00
14.50	6.231E+01	12.7	9.283E-02	15.97	5.156E+01	6.532E+00
14.75	7.428E+01	17.2	1.057E-01	16.25	6.148E+01	1.056E+01
15.00	1.153E+02	11.1	1.754E-01	16.52	9.546E+01	1.060E+01
15.25	1.273E+02	9.3	2.068E-01	16.80	1.054E+02	9.805E+00
15.50	1.643E+02	7.2	2.847E-01	17.07	1.361E+02	9.767E+00
15.75	1.759E+02	3.5	3.249E-01	17.35	1.457E+02	5.150E+00
16.00	1.890E+02	2.9	3.717E-01	17.62	1.566E+02	4.503E+00
16.25	1.974E+02	4.6	4.129E-01	17.90	1.636E+02	7.575E+00
16.39	1.932E+02	2.1	4.181E-01	18.05	1.602E+02	3.348E+00
16.89	1.756E+02	3.4	4.281E-01	18.60	1.456E+02	4.977E+00
17.39	1.437E+02	4.9	3.933E-01	19.15	1.192E+02	5.814E+00
18.00	1.118E+02	6.6	3.509E-01	19.82	9.282E+01	6.138E+00
18.50	7.661E+01	10.7	2.681E-01	20.37	6.365E+01	6.829E+00
19.00	4.341E+01	14.9	1.688E-01	20.92	3.608E+01	5.372E+00
19.50	2.284E+01	13.6	9.047E-02	21.46	1.900E+01	2.586E+00
20.00	1.765E+01	5.2	8.412E-02	22.01	1.469E+01	7.663E-01
20.50	1.983E+01	4.5	1.042E-01	22.56	1.651E+01	7.348E-01
21.00	2.464E+01	5.5	1.424E-01	23.11	2.053E+01	1.120E+00
21.50	3.069E+01	6.3	1.947E-01	23.66	2.559E+01	1.610E+00
22.00	4.052E+01	5.7	2.815E-01	24.20	3.380E+01	1.925E+00
22.39	4.767E+01	2.7	3.550E-01	24.63	3.979E+01	1.075E+00
22.89	4.677E+01	1.3	3.800E-01	25.18	3.906E+01	5.202E-01
23.39	4.326E+01	2.6	3.827E-01	25.73	3.615E+01	9.272E-01
24.00	3.682E+01	4.0	3.606E-01	26.39	3.080E+01	1.242E+00
24.50	3.014E+01	5.6	3.202E-01	26.94	2.523E+01	1.414E+00
25.00	2.288E+01	6.6	2.632E-01	27.49	1.917E+01	1.257E+00
25.50	1.778E+01	7.9	2.211E-01	28.03	1.490E+01	1.172E+00
26.00	1.145E+01	9.2	1.537E-01	28.58	9.607E+00	8.867E-01
26.50	9.072E+00	5.5	1.312E-01	29.13	7.616E+00	4.155E-01
27.00	7.536E+00	3.4	1.173E-01	29.67	6.332E+00	2.156E-01
27.50	7.424E+00	2.8	1.242E-01	30.22	6.242E+00	1.721E-01
28.00	8.691E+00	2.8	1.560E-01	30.76	7.314E+00	2.041E-01
28.50	9.070E+00	2.0	1.745E-01	31.31	7.639E+00	1.564E-01
29.00	9.804E+00	2.1	2.020E-01	31.85	8.264E+00	1.726E-01
29.39	9.461E+00	0.9	2.053E-01	32.28	7.980E+00	6.789E-02
29.89	9.427E+00	1.2	2.186E-01	32.82	7.958E+00	9.798E-02
30.39	8.736E+00	1.9	2.161E-01	33.37	7.381E+00	1.418E-01
31.00	7.938E+00	2.7	2.122E-01	34.03	6.714E+00	1.832E-01
31.50	6.832E+00	4.4	1.944E-01	34.57	5.784E+00	2.532E-01
32.00	5.497E+00	5.8	1.663E-01	35.12	4.658E+00	2.690E-01
32.50	4.201E+00	5.6	1.350E-01	35.66	3.563E+00	1.981E-01
33.00	3.576E+00	4.1	1.220E-01	36.20	3.036E+00	1.242E-01
33.50	3.047E+00	4.0	1.102E-01	36.75	2.589E+00	1.036E-01
34.00	2.585E+00	2.7	9.900E-02	37.29	2.198E+00	5.835E-02
34.50	2.646E+00	1.6	1.072E-01	37.83	2.252E+00	3.661E-02
35.00	2.760E+00	1.5	1.183E-01	38.38	2.352E+00	3.488E-02
35.50	2.922E+00	1.8	1.323E-01	38.92	2.493E+00	4.611E-02
36.00	3.126E+00	1.6	1.494E-01	39.46	2.669E+00	4.379E-02
36.50	3.099E+00	2.2	1.563E-01	40.00	2.649E+00	5.772E-02

SCATTERING OF 4-HE PARTICLES ON 40-CA

ELAB = 104.000 MEV Q = 0.0 MEV I = 0 +

ECM = 94.532 MEV K = 4.0567/FERMI ETA = 1.23581

(continued)

LABORATORY DATA THETA DEGREE	SIGMA MB/SR	DSIGMA %	RUTHERFORD SIGMA/SR	CM DATA THETA DEGREE	SIGMA MB/SR	DSIGMA MB/SR
36.89	3.482E+00	3.0	1.829E-01	40.42	2.978E+00	9.044E-02
37.39	3.208E+00	1.8	1.775E-01	40.96	2.747E+00	4.946E-02
37.89	3.190E+00	1.3	1.858E-01	41.50	2.735E+00	3.617E-02
38.50	3.220E+00	1.9	1.995E-01	42.16	2.764E+00	5.182E-02
39.00	2.942E+00	2.4	1.915E-01	42.70	2.528E+00	6.118E-02
39.50	2.732E+00	2.2	1.967E-01	43.24	2.350E+00	5.106E-02
40.00	2.547E+00	2.4	1.827E-01	43.78	2.194E+00	5.170E-02
40.50	2.409E+00	1.9	1.813E-01	44.32	2.077E+00	3.979E-02
41.00	2.344E+00	2.3	1.848E-01	44.86	2.023E+00	4.677E-02
41.50	2.069E+00	2.5	1.709E-01	45.40	1.798E+00	4.558E-02
42.00	2.048E+00	1.7	1.771E-01	45.94	1.772E+00	3.004E-02
42.50	2.107E+00	2.2	1.906E-01	46.48	1.825E+00	3.936E-02
42.89	1.937E+00	2.9	1.814E-01	46.90	1.679E+00	4.811E-02
43.39	2.036E+00	2.1	1.993E-01	47.43	1.767E+00	3.705E-02
43.89	2.107E+00	2.0	2.155E-01	47.97	1.831E+00	3.655E-02
44.50	2.049E+00	1.9	2.208E-01	48.62	1.783E+00	3.421E-02
45.00	2.082E+00	1.7	2.341E-01	49.16	1.814E+00	3.070E-02
45.50	2.074E+00	2.3	2.432E-01	49.70	1.809E+00	4.179E-02
46.00	1.821E+00	2.7	2.226E-01	50.23	1.591E+00	4.309E-02
46.80	1.736E+00	2.2	2.265E-01	51.09	1.520E+00	3.379E-02
47.80	1.494E+00	3.0	2.110E-01	52.16	1.311E+00	3.967E-02
48.80	1.377E+00	2.5	2.104E-01	53.23	1.212E+00	3.047E-02
49.80	1.329E+00	2.1	2.190E-01	54.29	1.172E+00	2.516E-02
50.80	1.154E+00	3.0	2.049E-01	55.36	1.021E+00	3.106E-02
51.80	1.048E+00	2.5	2.000E-01	56.42	9.291E-01	2.357E-02
52.80	9.681E-01	3.5	1.985E-01	57.49	8.610E-01	2.994E-02
53.80	8.429E-01	4.2	1.853E-01	58.55	7.518E-01	3.192E-02
54.80	7.605E-01	3.3	1.789E-01	59.61	6.802E-01	2.273E-02
55.80	6.402E-01	4.1	1.610E-01	60.67	5.742E-01	2.332E-02
56.80	5.286E-01	4.7	1.419E-01	61.72	4.750E-01	2.216E-02
57.80	4.627E-01	3.9	1.324E-01	62.78	4.175E-01	1.610E-02
58.80	4.025E-01	3.4	1.227E-01	63.83	3.643E-01	1.229E-02
59.80	3.414E-01	3.8	1.106E-01	64.89	3.099E-01	1.189E-02
60.80	2.988E-01	3.5	1.028E-01	65.94	2.720E-01	9.538E-03
61.80	2.638E-01	3.4	9.631E-02	66.99	2.410E-01	8.274E-03
62.80	2.231E-01	3.8	8.629E-02	68.03	2.044E-01	7.811E-03
63.80	1.833E-01	3.8	7.504E-02	69.08	1.685E-01	6.472E-03
64.80	1.494E-01	4.2	6.464E-02	70.12	1.377E-01	5.822E-03
65.80	1.290E-01	4.6	5.896E-02	71.17	1.193E-01	5.472E-03
66.80	1.096E-01	3.9	5.285E-02	72.21	1.017E-01	4.005E-03
67.80	8.381E-02	3.7	4.259E-02	73.25	7.802E-02	2.898E-03
68.80	7.372E-02	3.4	3.945E-02	74.29	6.885E-02	2.374E-03
69.80	6.150E-02	4.3	3.461E-02	75.32	5.763E-02	2.454E-03
70.80	4.957E-02	4.5	2.932E-02	76.36	4.660E-02	2.116E-03
73.30	3.628E-02	5.0	2.420E-02	78.93	3.440E-02	1.729E-03
75.80	2.231E-02	5.6	1.670E-02	81.50	2.133E-02	1.187E-03
78.30	1.494E-02	5.8	1.248E-02	84.06	1.441E-02	8.365E-04
80.80	1.290E-02	6.0	1.197E-02	86.61	1.255E-02	7.579E-04
83.30	7.091E-03	6.9	7.278E-03	89.14	6.961E-03	4.837E-04
85.80	5.141E-03	10.0	5.811E-03	91.66	5.092E-03	5.092E-04
88.30	2.813E-03	11.3	3.487E-03	94.18	2.811E-03	3.180E-04
90.80	2.250E-03	10.8	3.047E-03	96.68	2.269E-03	2.445E-04
95.80	9.089E-04	30.1	1.453E-03	101.65	9.332E-04	2.809E-04
100.80	4.704E-04	19.0	8.753E-04	106.57	4.917E-04	9.328E-05
102.80	2.522E-04	21.7	4.968E-04	108.53	2.655E-04	5.769E-05
110.80	8.730E-05	33.3	2.120E-04	116.29	9.449E-05	3.150E-05

SCATTERING OF 4-HE PARTICLES ON 42-CA

ELAB = 104.000 MEV Q = 0.0 MEV I = 0 +

ECM = 94.943 MEV K = 4.0744/FERMI ETA = 1.23581

LABORATORY DATA			RUTHERFORD	CM DATA		
THETA DEGREE	SIGMA MB/SR	DSIGMA %	SIGMA/SR	THETA DEGREE	SIGMA MB/SR	DSIGMA MB/SR
3.29	1.558E+05	6.7	5.544E-01	3.61	1.293E+05	8.673E+03
3.79	1.036E+05	8.2	6.491E-01	4.16	8.599E+04	7.028E+03
4.29	7.119E+04	7.9	7.321E-01	4.71	5.910E+04	4.653E+03
4.90	4.243E+04	9.1	7.425E-01	5.38	3.523E+04	3.222E+03
5.40	2.724E+04	10.7	7.029E-01	5.93	2.262E+04	2.427E+03
5.81	1.564E+04	13.3	5.422E-01	6.38	1.299E+04	1.722E+03
6.40	7.772E+03	14.2	3.954E-01	7.02	6.456E+03	9.161E+02
6.90	3.476E+03	18.2	2.388E-01	7.57	2.898E+03	5.266E+02
7.40	1.443E+03	19.2	1.311E-01	8.12	1.199E+03	2.300E+02
7.82	8.325E+02	9.4	9.434E-02	8.58	6.919E+02	6.531E+01
8.31	9.067E+02	4.4	1.167E-01	9.12	9.706E+02	2.964E+01
8.81	1.107E+03	8.4	2.018E-01	9.67	9.208E+02	7.714E+01
9.40	1.825E+03	3.7	4.312E-01	10.32	1.518E+03	5.559E+01
9.90	1.781E+03	1.3	5.174E-01	10.86	1.482E+03	1.920E+01
10.40	1.637E+03	2.2	5.787E-01	11.41	1.362E+03	2.994E+01
10.90	1.445E+03	4.7	6.162E-01	11.96	1.203E+03	5.653E+01
11.40	9.608E+02	8.8	4.899E-01	12.51	8.001E+02	7.058E+01
11.90	5.993E+02	11.8	3.626E-01	13.06	4.993E+02	5.871E+01
12.32	3.133E+02	16.9	2.175E-01	13.51	2.611E+02	4.421E+01
12.90	9.433E+01	28.3	7.872E-02	14.15	7.864E+01	2.226E+01
13.40	1.594E+01	57.0	1.547E-02	14.70	1.329E+01	7.572E+00
13.82	5.579E+00	35.4	6.133E-03	15.16	4.654E+00	1.650E+00
14.00	8.213E+00	65.0	9.493E-03	15.36	6.852E+00	4.455E+00
14.29	3.479E+01	25.1	4.363E-02	15.67	2.903E+01	7.291E+00
14.50	5.218E+01	20.5	6.936E-02	15.90	4.355E+01	8.931E+00
14.79	9.014E+01	13.4	1.296E-01	16.22	7.526E+01	1.011E+01
15.00	1.134E+02	12.7	1.725E-01	16.45	9.468E+01	1.202E+01
15.44	1.735E+02	6.1	2.962E-01	16.93	1.450E+02	8.899E+00
15.92	2.101E+02	2.0	4.050E-01	17.46	1.756E+02	3.593E+00
16.42	2.134E+02	1.7	4.649E-01	18.00	1.784E+02	3.115E+00
16.91	1.822E+02	3.3	4.463E-01	18.54	1.524E+02	5.092E+00
17.44	1.523E+02	5.3	4.220E-01	19.12	1.274E+02	6.804E+00
17.94	1.128E+02	9.6	3.494E-01	19.67	9.443E+01	9.064E+00
18.40	6.400E+01	12.0	2.191E-01	20.17	5.361E+01	6.413E+00
19.40	1.777E+01	17.3	7.504E-02	21.26	1.490E+01	2.575E+00
19.79	1.199E+01	7.4	5.478E-02	21.69	1.006E+01	7.450E-01
20.29	1.296E+01	5.8	6.539E-02	22.23	1.088E+01	6.269E-01
20.79	1.894E+01	10.6	1.052E-01	22.78	1.590E+01	1.685E+00
21.40	3.575E+01	6.4	2.226E-01	23.45	3.005E+01	1.924E+00
21.90	4.441E+01	3.0	3.030E-01	23.99	3.735E+01	1.113E+00
22.40	4.817E+01	1.5	3.593E-01	24.54	4.054E+01	5.937E-01
22.90	4.928E+01	1.7	4.010E-01	25.08	4.150E+01	7.110E-01
23.40	4.414E+01	2.9	3.912E-01	25.63	3.719E+01	1.081E+00
23.90	3.742E+01	5.1	3.605E-01	26.17	3.155E+01	1.597E+00
24.40	2.584E+01	7.3	2.700E-01	26.72	2.180E+01	1.599E+00
24.90	1.886E+01	6.8	2.135E-01	27.26	1.593E+01	1.080E+00
25.40	1.340E+01	6.7	1.640E-01	27.80	1.132E+01	7.638E-01
26.00	9.603E+00	6.0	1.289E-01	28.46	8.121E+00	4.869E-01
26.50	7.488E+00	4.3	1.083E-01	29.00	6.337E+00	2.699E-01
27.00	7.004E+00	2.9	1.090E-01	29.54	5.931E+00	1.705E-01
27.29	6.949E+00	2.9	1.128E-01	29.86	5.887E+00	1.724E-01
27.50	7.584E+00	2.8	1.268E-01	30.09	6.427E+00	1.820E-01
27.79	7.747E+00	3.3	1.350E-01	30.40	6.569E+00	2.170E-01
28.00	8.489E+00	3.3	1.524E-01	30.63	7.200E+00	2.370E-01
28.29	8.845E+00	2.5	1.653E-01	30.95	7.506E+00	1.906E-01
28.50	9.342E+00	3.1	1.797E-01	31.17	7.929E+00	2.464E-01
28.90	1.049E+01	2.1	2.132E-01	31.61	8.912E+00	1.898E-01
29.40	1.020E+01	1.6	2.216E-01	32.15	8.669E+00	1.421E-01
29.90	1.010E+01	2.0	2.344E-01	32.69	8.592E+00	1.735E-01
30.40	8.643E+00	3.5	2.140E-01	33.24	7.358E+00	2.597E-01
30.90	7.378E+00	3.9	1.947E-01	33.78	6.287E+00	2.454E-01
31.40	6.177E+00	5.2	1.736E-01	34.32	5.268E+00	2.749E-01
31.90	4.351E+00	6.2	1.300E-01	34.86	3.714E+00	2.313E-01
32.40	3.626E+00	5.0	1.151E-01	35.40	3.098E+00	1.556E-01
32.90	2.804E+00	4.3	9.451E-02	35.94	2.398E+00	1.040E-01
33.29	2.669E+00	1.7	9.417E-02	36.37	2.284E+00	3.886E-02
33.79	2.581E+00	1.6	9.651E-02	36.91	2.211E+00	3.485E-02
34.29	2.621E+00	2.0	1.037E-01	37.45	2.247E+00	4.595E-02
34.90	3.069E+00	2.0	1.301E-01	38.11	2.634E+00	5.379E-02
35.40	3.212E+00	1.5	1.438E-01	38.65	2.759E+00	4.257E-02
35.90	3.367E+00	1.2	1.592E-01	39.19	2.896E+00	3.434E-02
36.40	3.353E+00	1.2	1.672E-01	39.73	2.896E+00	3.524E-02
36.90	3.347E+00	1.5	1.760E-01	40.27	2.884E+00	4.202E-02
37.40	3.131E+00	1.7	1.734E-01	40.80	2.700E+00	4.711E-02
37.90	2.949E+00	1.7	1.719E-01	41.34	2.546E+00	4.206E-02
38.40	2.773E+00	2.0	1.700E-01	41.88	2.396E+00	4.720E-02
38.90	2.522E+00	2.8	1.625E-01	42.42	2.182E+00	6.028E-02
39.50	2.062E+00	3.1	1.409E-01	43.07	1.786E+00	5.618E-02
40.00	1.867E+00	2.0	1.339E-01	43.60	1.619E+00	3.254E-02
40.50	1.902E+00	1.7	1.430E-01	44.14	1.651E+00	2.852E-02
40.79	1.811E+00	2.1	1.400E-01	44.45	1.573E+00	3.233E-02

SCATTERING OF 4-HE PARTICLES ON 42-CA

ELAB = 104.000 MEV Q = 0.0 MEV I = 0 +

ECM = 94.943 MEV K = 4.0744/FERMI ETA = 1.23581

(continued)

LABORATORY DATA THETA DEGREE	SIGMA MB/SR	DSIGMA %	RUTHERFORD SIGMA/SR	CM DATA THETA DEGREE	SIGMA MB/SR	DSIGMA MB/SR
41.00	1.845E+00	1.5	1.455E-01	44.68	1.603E+00	2.407E-02
41.29	1.850E+00	1.6	1.499E-01	44.99	1.609E+00	2.635E-02
41.50	1.886E+00	1.6	1.558E-01	45.21	1.641E+00	2.609E-02
41.79	1.854E+00	1.8	1.573E-01	45.53	1.614E+00	2.953E-02
42.00	1.800E+00	2.2	1.556E-01	45.75	1.568E+00	3.431E-02
42.40	1.936E+00	1.7	1.736E-01	46.18	1.688E+00	2.868E-02
42.90	1.923E+00	1.4	1.803E-01	46.72	1.678E+00	2.379E-02
43.40	1.935E+00	1.4	1.896E-01	47.25	1.690E+00	2.356E-02
43.90	1.932E+00	1.8	1.977E-01	47.79	1.690E+00	3.016E-02
44.40	1.751E+00	2.0	1.871E-01	48.32	1.533E+00	3.027E-02
44.90	1.727E+00	2.1	1.926E-01	48.86	1.514E+00	3.166E-02
45.40	1.515E+00	2.4	1.761E-01	49.39	1.330E+00	3.215E-02
45.90	1.451E+00	2.0	1.758E-01	49.93	1.275E+00	2.612E-02
46.40	1.332E+00	2.9	1.682E-01	50.46	1.172E+00	3.347E-02
46.79	1.184E+00	2.7	1.543E-01	50.88	1.043E+00	2.794E-02
47.29	1.142E+00	2.1	1.549E-01	51.41	1.007E+00	2.145E-02
47.79	1.029E+00	2.3	1.452E-01	51.94	9.082E-01	2.122E-02
48.40	9.827E-01	2.1	1.455E-01	52.59	8.688E-01	1.822E-02
48.90	9.460E-01	2.0	1.456E-01	53.12	8.374E-01	1.686E-02
49.40	8.903E-01	2.0	1.423E-01	53.66	7.890E-01	1.576E-02
49.90	8.927E-01	2.4	1.482E-01	54.19	7.922E-01	1.885E-02
50.40	8.144E-01	2.3	1.403E-01	54.72	7.236E-01	1.700E-02
50.90	7.974E-01	2.4	1.426E-01	55.25	7.094E-01	1.672E-02
51.40	7.358E-01	2.5	1.364E-01	55.78	6.554E-01	1.645E-02
51.90	7.003E-01	2.4	1.346E-01	56.31	6.247E-01	1.505E-02
52.40	6.333E-01	3.0	1.262E-01	56.84	5.656E-01	1.714E-02
52.69	6.727E-01	2.5	1.368E-01	57.15	6.012E-01	1.513E-02
53.29	6.124E-01	3.4	1.299E-01	57.78	5.482E-01	1.851E-02
53.79	5.020E-01	3.1	1.102E-01	58.31	4.501E-01	1.408E-02
54.30	5.246E-01	2.4	1.193E-01	58.85	4.710E-01	1.118E-02
54.90	4.820E-01	2.8	1.141E-01	59.49	4.334E-01	1.231E-02
55.40	4.367E-01	2.3	1.069E-01	60.01	3.932E-01	9.192E-03
55.83	4.155E-01	2.5	1.047E-01	60.46	3.746E-01	9.274E-03
56.40	3.990E-01	3.2	1.044E-01	61.07	3.603E-01	1.156E-02
56.90	3.447E-01	2.6	9.312E-02	61.60	3.116E-01	8.221E-03
57.32	3.422E-01	2.8	9.497E-02	62.04	3.098E-01	8.739E-03
57.90	3.032E-01	4.1	8.730E-02	62.65	2.749E-01	1.119E-02
58.40	2.473E-01	3.6	7.349E-02	63.17	2.245E-01	8.168E-03
58.81	2.595E-01	3.3	7.909E-02	63.60	2.359E-01	7.848E-03
59.29	2.240E-01	3.6	7.035E-02	64.11	2.039E-01	7.352E-03
59.79	1.972E-01	2.8	6.384E-02	64.63	1.798E-01	5.091E-03
60.40	1.958E-01	2.8	6.578E-02	65.27	1.788E-01	5.068E-03
60.90	1.746E-01	3.0	6.043E-02	65.80	1.597E-01	4.837E-03
61.40	1.650E-01	3.0	5.883E-02	66.32	1.512E-01	4.603E-03
61.90	1.494E-01	3.8	5.485E-02	66.84	1.371E-01	5.272E-03
62.40	1.327E-01	3.3	5.013E-02	67.37	1.219E-01	4.048E-03
62.90	1.332E-01	3.4	5.178E-02	67.89	1.225E-01	4.112E-03
63.40	1.179E-01	3.5	4.718E-02	68.41	1.086E-01	3.769E-03
63.90	1.145E-01	3.4	4.712E-02	68.93	1.057E-01	3.544E-03
64.40	9.762E-02	4.1	4.131E-02	69.45	9.021E-02	3.703E-03
66.29	6.935E-02	3.3	3.253E-02	71.42	6.446E-02	2.104E-03
69.40	4.848E-02	4.2	2.673E-02	74.65	4.550E-02	1.922E-03
70.90	2.000E-02	8.2	1.199E-02	76.19	1.886E-02	1.545E-03
72.29	2.641E-02	5.1	1.679E-02	77.63	2.501E-02	1.272E-03
73.90	2.220E-02	5.0	1.524E-02	79.28	2.116E-02	1.056E-03
75.40	1.697E-02	6.3	1.247E-02	80.82	1.624E-02	1.022E-03
76.90	1.123E-02	7.6	8.821E-03	82.36	1.080E-02	8.184E-04
78.29	8.176E-03	7.3	6.825E-03	83.78	7.898E-03	5.762E-04
81.40	5.760E-03	8.4	5.476E-03	86.94	5.622E-03	4.730E-04
82.90	3.421E-03	10.8	3.454E-03	88.46	3.356E-03	3.615E-04
84.29	3.477E-03	8.9	3.708E-03	89.86	3.427E-03	3.066E-04
85.90	3.079E-03	9.1	3.491E-03	91.49	3.051E-03	2.775E-04
87.40	2.226E-03	11.5	2.669E-03	93.00	2.217E-03	2.551E-04
88.90	1.497E-03	13.5	1.895E-03	94.50	1.499E-03	2.027E-04
91.79	7.673E-04	18.2	1.074E-03	97.39	7.759E-04	1.413E-04
93.40	7.162E-04	16.5	1.058E-03	98.99	7.282E-04	1.200E-04
94.90	2.395E-04	40.5	3.717E-04	100.48	2.448E-04	9.910E-05
96.40	4.667E-04	20.8	7.596E-04	101.96	4.794E-04	9.953E-05
102.40	1.823E-04	34.3	3.549E-04	107.87	1.912E-04	6.561E-05
103.90	2.560E-05	133.3	5.196E-05	109.33	2.698E-05	3.597E-05

SCATTERING OF 4-HE PARTICLES ON 44-CA

ELAB = 104.000 MEV Q = 0.0 MEV I = 0 +

ECM = 95.320 MEV K = 4.0906/FERMI ETA = 1.23581

LABORATORY DATA			RUTHERFORD	CM DATA		
THETA DEGREE	SIGMA MB/SR	DSIGMA %	SIGMA/SR	THETA DEGREE	SIGMA MB/SR	DSIGMA MB/SR
3.29	1.474E+05	7.1	5.246E-01	3.60	1.234E+05	8.753E+03
3.79	9.518E+04	8.3	5.963E-01	4.14	7.964E+04	6.638E+03
4.29	6.818E+04	7.5	7.011E-01	4.69	5.706E+04	4.282E+03
4.84	4.189E+04	9.3	6.952E-01	5.29	3.506E+04	3.271E+03
5.33	2.697E+04	9.4	6.623E-01	5.83	2.257E+04	2.127E+03
5.84	1.650E+04	11.1	5.807E-01	6.38	1.381E+04	1.538E+03
6.40	7.556E+03	16.2	3.844E-01	7.00	6.328E+03	1.027E+03
6.90	3.241E+03	19.0	2.227E-01	7.54	2.715E+03	5.168E+02
7.40	1.397E+03	17.7	1.269E-01	8.09	1.170E+03	2.071E+02
7.81	8.873E+02	7.3	1.002E-01	8.54	7.434E+02	5.426E+01
8.31	9.003E+02	4.6	1.301E-01	9.08	7.545E+02	3.452E+01
8.81	1.260E+03	8.1	2.295E-01	9.63	1.056E+03	8.517E+01
9.40	2.011E+03	4.1	4.749E-01	10.27	1.686E+03	6.935E+01
9.90	1.833E+03	2.1	5.325E-01	10.82	1.538E+03	3.240E+01
10.40	1.656E+03	2.3	5.856E-01	11.37	1.390E+03	3.232E+01
10.90	1.477E+03	5.0	6.297E-01	11.91	1.240E+03	6.203E+01
11.40	9.214E+02	10.1	4.698E-01	12.46	7.735E+02	7.804E+01
11.90	5.495E+02	12.7	3.324E-01	13.00	4.614E+02	5.868E+01
12.32	2.777E+02	18.0	1.927E-01	13.46	2.333E+02	4.196E+01
12.90	7.614E+01	27.3	6.353E-02	14.09	6.398E+01	1.746E+01
13.83	1.188E+01	41.5	1.308E-02	15.11	9.991E+00	4.142E+00
14.00	1.687E+01	45.5	1.949E-02	15.29	1.418E+01	6.451E+00
14.29	5.281E+01	20.6	6.623E-02	15.61	4.442E+01	9.142E+00
14.50	7.236E+01	16.1	9.616E-02	15.84	6.087E+01	9.827E+00
14.79	1.130E+02	11.8	1.625E-01	16.16	9.510E+01	1.118E+01
15.00	1.393E+02	9.2	2.118E-01	16.38	1.172E+02	1.073E+01
15.44	1.959E+02	4.5	3.339E-01	16.86	1.649E+02	7.436E+00
15.95	2.198E+02	1.2	4.268E-01	17.42	1.851E+02	2.186E+00
16.41	2.186E+02	2.0	4.756E-01	17.93	1.842E+02	3.636E+00
16.91	1.797E+02	4.1	4.400E-01	18.47	1.515E+02	6.261E+00
17.44	1.442E+02	6.5	3.988E-01	19.04	1.216E+02	7.942E+00
17.94	9.813E+01	10.8	3.033E-01	19.59	8.280E+01	8.930E+00
18.40	5.622E+01	11.6	1.925E-01	20.09	4.746E+01	5.499E+00
19.40	1.775E+01	15.4	7.494E-02	21.18	1.500E+01	2.315E+00
19.79	1.157E+01	10.3	5.287E-02	21.60	9.783E+00	1.006E+00
20.29	1.526E+01	8.2	7.694E-02	22.15	1.290E+01	1.061E+00
20.79	2.367E+01	9.9	1.315E-01	22.69	2.004E+01	1.975E+00
21.40	4.139E+01	5.0	2.577E-01	23.35	3.505E+01	1.765E+00
21.90	4.722E+01	2.2	3.221E-01	23.90	4.001E+01	8.785E-01
22.40	5.035E+01	1.5	3.755E-01	24.44	4.269E+01	6.491E-01
22.90	4.836E+01	1.8	3.934E-01	24.98	4.102E+01	7.387E-01
23.40	4.335E+01	3.6	3.841E-01	25.53	3.680E+01	1.325E+00
23.90	3.371E+01	6.1	3.246E-01	26.07	2.863E+01	1.742E+00
24.40	2.346E+01	7.7	2.451E-01	26.61	1.994E+01	1.529E+00
24.90	1.603E+01	7.5	1.814E-01	27.15	1.363E+01	1.025E+00
25.40	1.180E+01	6.2	1.444E-01	27.70	1.004E+01	6.261E-01
26.00	8.691E+00	4.9	1.166E-01	28.35	7.403E+00	3.649E-01
26.50	7.495E+00	3.3	1.084E-01	28.89	6.389E+00	2.092E-01
27.00	7.651E+00	2.9	1.190E-01	29.43	6.526E+00	1.873E-01
27.29	7.605E+00	3.8	1.234E-01	29.74	6.490E+00	2.434E-01
27.50	8.413E+00	3.8	1.407E-01	29.97	7.181E+00	2.699E-01
27.79	8.746E+00	3.9	1.524E-01	30.28	7.469E+00	2.895E-01
28.00	9.639E+00	3.0	1.730E-01	30.51	8.234E+00	2.503E-01
28.29	9.673E+00	2.1	1.808E-01	30.83	8.267E+00	1.724E-01
28.50	1.021E+01	2.8	1.965E-01	31.05	8.731E+00	2.453E-01
28.90	1.118E+01	2.9	2.272E-01	31.49	9.567E+00	2.764E-01
29.40	1.010E+01	2.5	2.195E-01	32.03	8.647E+00	2.192E-01
29.90	9.627E+00	2.5	2.234E-01	32.57	8.247E+00	2.075E-01
30.40	8.117E+00	4.3	2.010E-01	33.11	6.960E+00	3.018E-01
30.90	6.792E+00	5.1	1.792E-01	33.65	5.828E+00	2.956E-01
31.40	5.174E+00	6.2	1.454E-01	34.19	4.443E+00	2.751E-01
31.90	3.782E+00	6.8	1.130E-01	34.73	3.251E+00	2.226E-01
32.40	2.948E+00	5.3	9.358E-02	35.27	2.536E+00	1.353E-01
32.90	2.649E+00	3.1	8.927E-02	35.81	2.281E+00	7.125E-02
33.29	2.569E+00	2.5	9.064E-02	36.23	2.214E+00	5.621E-02
33.79	2.558E+00	1.6	9.561E-02	36.77	2.205E+00	3.600E-02
34.29	2.681E+00	1.9	1.061E-01	37.30	2.313E+00	4.430E-02
34.90	2.972E+00	2.7	1.259E-01	37.96	2.568E+00	7.045E-02
35.40	3.240E+00	1.7	1.451E-01	38.50	2.802E+00	4.774E-02
35.90	3.342E+00	1.8	1.580E-01	39.04	2.893E+00	5.140E-02
36.40	2.981E+00	2.7	1.486E-01	39.58	2.582E+00	6.989E-02
36.90	2.923E+00	2.1	1.537E-01	40.11	2.535E+00	5.343E-02
37.40	2.529E+00	3.2	1.400E-01	40.65	2.195E+00	7.058E-02
37.90	2.194E+00	3.7	1.279E-01	41.19	1.906E+00	7.048E-02
38.40	1.929E+00	2.6	1.182E-01	41.72	1.677E+00	4.426E-02
38.90	1.794E+00	2.5	1.156E-01	42.26	1.562E+00	3.951E-02

SCATTERING OF 4-HE PARTICLES ON 44-CA

ELAB = 104.000 MEV Q = 0.0 MEV I = 0 +

ECM = 95.320 MEV K = 4.0906/FERMI ETA = 1.23581

(continued)

LABORATORY DATA			RUTHERFORD	CM DATA		
THETA DEGREE	SIGMA MB/SR	DSIGMA %	SIGMA/SR	THETA DEGREE	SIGMA MB/SR	DSIGMA MB/SR
39.50	1.520E+00	3.5	1.038E-01	42.90	1.324E+00	4.656E-02
40.00	1.578E+00	1.8	1.132E-01	43.44	1.377E+00	2.539E-02
40.50	1.561E+00	1.6	1.174E-01	43.98	1.363E+00	2.189E-02
40.79	1.566E+00	1.7	1.211E-01	44.29	1.369E+00	2.389E-02
41.00	1.584E+00	1.9	1.249E-01	44.51	1.385E+00	2.607E-02
41.29	1.509E+00	2.0	1.222E-01	44.82	1.320E+00	2.647E-02
41.50	1.522E+00	1.9	1.257E-01	45.05	1.332E+00	2.489E-02
41.79	1.598E+00	2.2	1.355E-01	45.36	1.399E+00	3.080E-02
42.00	1.554E+00	2.5	1.343E-01	45.58	1.361E+00	3.393E-02
42.40	1.717E+00	2.2	1.538E-01	46.01	1.505E+00	3.359E-02
42.90	1.637E+00	1.6	1.534E-01	46.54	1.437E+00	2.312E-02
43.40	1.626E+00	1.5	1.592E-01	47.08	1.429E+00	2.147E-02
43.90	1.627E+00	2.0	1.665E-01	47.61	1.431E+00	2.800E-02
44.40	1.459E+00	2.4	1.559E-01	48.14	1.285E+00	3.087E-02
44.90	1.382E+00	2.3	1.541E-01	48.68	1.219E+00	2.794E-02
45.40	1.254E+00	2.7	1.458E-01	49.21	1.107E+00	2.935E-02
45.90	1.133E+00	2.1	1.373E-01	49.74	1.001E+00	2.147E-02
46.40	1.122E+00	2.4	1.416E-01	50.27	9.924E-01	2.402E-02
46.79	9.881E-01	3.6	1.287E-01	50.69	8.749E-01	3.136E-02
47.29	8.778E-01	2.7	1.191E-01	51.22	7.781E-01	2.085E-02
47.79	8.678E-01	2.7	1.224E-01	51.75	7.701E-01	2.085E-02
48.40	7.931E-01	2.7	1.174E-01	52.40	7.048E-01	1.868E-02
48.90	7.613E-01	2.7	1.171E-01	52.93	6.774E-01	1.327E-02
49.40	7.038E-01	3.0	1.125E-01	53.46	6.270E-01	1.878E-02
49.90	6.914E-01	2.8	1.148E-01	53.99	6.167E-01	1.731E-02
50.40	6.605E-01	2.9	1.138E-01	54.52	5.898E-01	1.693E-02
50.90	6.502E-01	3.3	1.162E-01	55.05	5.813E-01	1.928E-02
51.40	5.948E-01	2.8	1.103E-01	55.58	5.325E-01	1.473E-02
51.90	5.904E-01	2.8	1.135E-01	56.11	5.292E-01	1.459E-02
52.40	5.346E-01	3.4	1.065E-01	56.64	4.798E-01	1.633E-02
52.79	5.568E-01	2.3	1.140E-01	57.05	5.002E-01	1.172E-02
53.29	5.288E-01	3.4	1.121E-01	57.58	4.757E-01	1.601E-02
53.79	4.457E-01	2.6	9.784E-02	58.11	4.014E-01	1.063E-02
54.40	4.367E-01	2.5	9.996E-02	58.75	3.940E-01	9.853E-03
54.90	4.004E-01	3.2	9.480E-02	59.28	3.617E-01	1.166E-02
55.40	3.809E-01	2.2	9.325E-02	59.80	3.445E-01	7.519E-03
55.90	3.517E-01	3.3	8.999E-02	60.33	3.185E-01	1.046E-02
56.40	3.173E-01	3.8	8.296E-02	60.86	2.877E-01	1.106E-02
56.90	3.036E-01	2.4	8.209E-02	61.38	2.757E-01	6.538E-03
57.40	2.846E-01	3.1	7.937E-02	61.91	2.588E-01	8.052E-03
57.90	2.587E-01	3.7	7.449E-02	62.43	2.356E-01	8.823E-03
58.40	2.472E-01	2.7	7.343E-02	62.96	2.254E-01	6.121E-03
58.79	2.233E-01	3.6	6.798E-02	63.37	2.038E-01	7.246E-03
59.29	1.949E-01	3.2	6.117E-02	63.89	1.781E-01	5.683E-03
59.79	1.849E-01	2.7	5.986E-02	64.41	1.693E-01	4.643E-03
60.40	1.750E-01	3.1	5.878E-02	65.05	1.605E-01	4.975E-03
60.90	1.561E-01	3.3	5.402E-02	65.57	1.433E-01	4.775E-03
61.40	1.471E-01	3.2	5.241E-02	66.10	1.352E-01	4.305E-03
61.90	1.360E-01	3.6	4.991E-02	66.62	1.252E-01	4.483E-03
62.40	1.273E-01	3.8	4.807E-02	67.14	1.173E-01	4.470E-03
62.90	1.123E-01	3.8	4.367E-02	67.66	1.037E-01	3.919E-03
63.40	1.121E-01	3.2	4.484E-02	68.18	1.036E-01	3.328E-03
63.90	1.030E-01	3.9	4.237E-02	68.70	9.535E-02	3.721E-03
64.40	8.952E-02	4.1	3.787E-02	69.22	8.301E-02	3.429E-03
66.29	6.336E-02	3.4	2.971E-02	71.19	5.908E-02	1.996E-03
67.90	5.856E-02	3.1	2.989E-02	72.86	5.486E-02	1.697E-03
69.40	4.468E-02	4.1	2.463E-02	74.41	4.204E-02	1.740E-03
70.90	3.105E-02	4.7	1.844E-02	75.95	2.935E-02	1.371E-03
72.29	2.432E-02	4.7	1.545E-02	77.39	2.309E-02	1.092E-03
73.90	2.183E-02	4.6	1.497E-02	79.04	2.083E-02	9.565E-04
75.40	1.515E-02	6.1	1.113E-02	80.58	1.452E-02	8.920E-04
76.90	1.025E-02	6.9	8.049E-03	82.11	9.870E-03	6.855E-04
78.29	7.679E-03	7.2	6.407E-03	83.53	7.428E-03	5.322E-04
79.90	7.267E-03	6.6	6.491E-03	85.17	7.065E-03	4.669E-04
81.40	5.589E-03	8.3	5.311E-03	86.69	5.460E-03	4.529E-04
82.90	3.472E-03	10.1	3.504E-03	88.21	3.408E-03	3.436E-04
84.29	3.147E-03	9.9	3.353E-03	89.61	3.103E-03	3.060E-04
85.90	2.658E-03	9.8	3.013E-03	91.23	2.635E-03	2.579E-04
87.40	1.848E-03	12.8	2.214E-03	92.74	1.840E-03	2.349E-04
88.90	1.506E-03	13.2	1.906E-03	94.25	1.508E-03	1.998E-04
91.79	4.606E-04	26.7	6.445E-04	97.13	4.654E-04	1.243E-04
93.40	7.907E-04	17.4	1.168E-03	98.74	8.032E-04	1.394E-04
94.90	1.578E-04	76.4	2.446E-04	100.23	1.610E-04	1.231E-04
96.40	3.494E-04	25.6	5.683E-04	101.71	3.584E-04	9.170E-05
99.29	1.168E-04	45.5	2.075E-04	104.56	1.209E-04	5.509E-05
100.90	2.480E-04	30.0	4.620E-04	106.15	2.581E-04	7.749E-05
102.40	2.664E-05	127.9	5.180E-05	107.62	2.786E-05	3.565E-05
103.90	2.458E-05	185.6	4.984E-05	109.09	2.583E-05	4.795E-05

SCATTERING OF 4-HE PARTICLES ON 48-CA

ELAB = 104.000 MEV Q = 0.0 MEV I = 0 +

ECM = 95.988 MEV K = 4.1192/FERMI ETA = 1.23581

LABORATORY DATA			RUTHERFORD	CM DATA		
THETA DEGREE	SIGMA MB/SR	DSIGMA %	SIGMA/SR	THETA DEGREE	SIGMA MB/SR	DSIGMA MB/SR
2.89	3.115E+05	9.4	6.597E-01	3.14	2.643E+05	2.482E+04
3.39	1.658E+05	11.6	6.647E-01	3.68	1.407E+05	1.632E+04
4.41	7.215E+04	10.4	8.304E-01	4.79	6.125E+04	6.366E+03
4.91	4.333E+04	10.5	7.646E-01	5.33	3.678E+04	3.880E+03
5.39	2.749E+04	10.3	7.038E-01	5.85	2.334E+04	2.415E+03
6.00	1.312E+04	15.3	5.154E-01	6.51	1.114E+04	1.702E+03
6.50	5.034E+03	22.3	2.724E-01	7.06	4.276E+03	9.543E+02
7.00	2.003E+03	19.4	1.457E-01	7.60	1.702E+03	3.302E+02
7.50	1.199E+03	9.6	1.149E-01	8.14	1.019E+03	9.741E+01
8.00	1.190E+03	6.6	1.476E-01	8.68	1.012E+03	6.633E+01
8.50	1.595E+03	5.7	2.519E-01	9.23	1.355E+03	7.765E+01
9.00	1.866E+03	5.1	3.704E-01	9.77	1.587E+03	8.134E+01
9.50	2.066E+03	4.0	5.089E-01	10.31	1.757E+03	6.966E+01
10.00	1.901E+03	4.5	5.746E-01	10.85	1.617E+03	7.250E+01
10.39	1.562E+03	4.7	5.499E-01	11.27	1.329E+03	6.198E+01
10.89	1.274E+03	5.1	5.410E-01	11.82	1.084E+03	5.525E+01
11.39	9.155E+02	8.3	4.650E-01	12.36	7.793E+02	6.440E+01
12.00	4.324E+02	14.9	2.704E-01	13.02	3.682E+02	5.498E+01
12.50	1.841E+02	21.6	1.355E-01	13.56	1.569E+02	3.381E+01
13.00	3.605E+01	42.8	3.101E-02	14.10	3.072E+01	1.315E+01
13.50	3.014E+01	13.0	3.013E-02	14.65	2.569E+01	3.343E+00
14.00	6.143E+01	17.3	7.098E-02	15.19	5.238E+01	9.070E+00
14.50	1.357E+02	12.3	1.803E-01	15.73	1.158E+02	1.427E+01
14.75	1.816E+02	7.9	2.582E-01	16.00	1.549E+02	1.222E+01
15.00	2.065E+02	3.4	3.139E-01	16.27	1.762E+02	5.925E+00
15.25	2.131E+02	2.7	3.459E-01	16.54	1.818E+02	4.831E+00
15.50	2.326E+02	2.7	4.028E-01	16.81	1.985E+02	5.312E+00
15.75	2.419E+02	1.5	4.466E-01	17.08	2.066E+02	3.148E+00
16.00	2.418E+02	1.1	4.751E-01	17.35	2.065E+02	2.170E+00
16.25	2.439E+02	6.5	5.096E-01	17.62	2.083E+02	1.358E+01
16.39	2.246E+02	4.8	4.857E-01	17.77	1.919E+02	9.294E+00
16.89	1.860E+02	5.5	4.533E-01	18.32	1.590E+02	8.793E+00
17.39	1.234E+02	8.3	3.376E-01	18.86	1.055E+02	8.732E+00
18.00	7.658E+01	9.6	2.402E-01	19.52	6.550E+01	6.296E+00
18.50	4.197E+01	13.7	1.463E-01	20.06	3.592E+01	4.919E+00
19.00	1.970E+01	12.9	7.655E-02	20.60	1.686E+01	2.168E+00
19.50	1.725E+01	7.2	7.429E-02	21.14	1.477E+01	1.061E+00
20.00	2.619E+01	9.2	1.247E-01	21.68	2.245E+01	2.062E+00
20.50	4.027E+01	6.0	2.115E-01	22.22	3.453E+01	2.063E+00
21.00	4.875E+01	4.1	2.816E-01	22.76	4.182E+01	1.730E+00
21.50	5.900E+01	3.1	3.741E-01	23.30	5.064E+01	1.587E+00
22.00	6.455E+01	2.3	4.482E-01	23.84	5.543E+01	1.262E+00
22.89	5.490E+01	3.2	4.450E-01	24.80	4.719E+01	1.523E+00
23.39	4.488E+01	4.6	3.968E-01	25.34	3.860E+01	1.776E+00
24.50	2.402E+01	6.5	2.550E-01	26.53	2.069E+01	1.350E+00
25.00	1.867E+01	4.8	2.146E-01	27.07	1.609E+01	7.749E-01
26.00	1.345E+01	3.8	1.804E-01	28.15	1.161E+01	4.446E-01
26.50	1.373E+01	3.1	1.984E-01	28.69	1.185E+01	3.632E-01
27.50	1.653E+01	3.1	2.763E-01	29.77	1.429E+01	4.386E-01
28.00	1.772E+01	2.5	3.180E-01	30.30	1.533E+01	3.828E-01
28.50	1.838E+01	2.6	3.535E-01	30.84	1.591E+01	4.153E-01
29.00	1.759E+01	2.9	3.622E-01	31.38	1.524E+01	4.360E-01
29.39	1.583E+01	3.1	3.433E-01	31.80	1.372E+01	4.320E-01
29.89	1.396E+01	4.1	3.235E-01	32.33	1.211E+01	4.981E-01
30.39	1.079E+01	4.8	2.668E-01	32.87	9.366E+00	4.460E-01
31.00	8.683E+00	4.3	2.320E-01	33.53	7.543E+00	3.212E-01
31.50	7.248E+00	5.8	2.061E-01	34.06	6.302E+00	3.640E-01
32.00	4.926E+00	6.5	1.489E-01	34.60	4.286E+00	2.767E-01
32.50	4.347E+00	3.9	1.396E-01	35.14	3.785E+00	1.477E-01
33.00	4.070E+00	4.2	1.387E-01	35.67	3.547E+00	1.476E-01
33.50	3.553E+00	3.9	1.284E-01	36.21	3.098E+00	1.219E-01
34.00	3.981E+00	4.0	1.524E-01	36.74	3.474E+00	1.399E-01
34.50	3.452E+00	4.4	1.398E-01	37.28	3.015E+00	1.324E-01
34.94	3.717E+00	1.9	1.581E-01	37.75	3.249E+00	6.027E-02
35.43	3.719E+00	2.2	1.670E-01	38.27	3.254E+00	7.170E-02
35.93	3.476E+00	3.0	1.648E-01	38.81	3.044E+00	9.189E-02
36.43	3.009E+00	3.5	1.505E-01	39.34	2.637E+00	9.255E-02
36.89	2.678E+00	4.1	1.406E-01	39.84	2.348E+00	9.516E-02
37.39	2.061E+00	5.6	1.140E-01	40.37	1.809E+00	1.009E-01
37.89	1.638E+00	4.2	9.540E-02	40.91	1.439E+00	6.071E-02
38.40	1.455E+00	4.1	8.917E-02	41.45	1.280E+00	5.227E-02
38.96	1.379E+00	2.8	8.933E-02	42.04	1.214E+00	3.409E-02

SCATTERING OF 4-HE PARTICLES ON 48-CA

ELAB = 104.000 MEV Q = 0.0 MEV I = 0 +

ECM = 95.988 MEV K = 4.1192/FERMI ETA = 1.2356

(continued)

LABORATORY DATA THETA DEGREE	SIGMA MB/SR	DSIGMA %	RUTHERFORD SIGMA/SR	CM DATA THETA DEGREE	SIGMA MB/SR	DSIGMA MB/SR
39.50	1.339E+00	2.5	9.143E-02	42.62	1.179E+00	2.905E-02
40.00	1.502E+00	2.8	1.077E-01	43.15	1.325E+00	3.685E-02
40.50	1.448E+00	2.4	1.089E-01	43.69	1.279E+00	3.127E-02
41.00	1.527E+00	1.8	1.203E-01	44.22	1.350E+00	2.468E-02
41.50	1.551E+00	1.8	1.280E-01	44.75	1.372E+00	2.450E-02
42.00	1.627E+00	2.4	1.406E-01	45.28	1.441E+00	3.400E-02
42.44	1.771E+00	2.4	1.592E-01	45.75	1.570E+00	3.777E-02
42.90	1.622E+00	2.3	1.519E-01	46.24	1.438E+00	3.329E-02
43.40	1.557E+00	2.0	1.524E-01	46.77	1.382E+00	2.827E-02
43.90	1.503E+00	2.0	1.537E-01	47.30	1.335E+00	2.721E-02
44.44	1.451E+00	2.2	1.555E-01	47.88	1.291E+00	2.815E-02
44.95	1.334E+00	2.4	1.493E-01	48.41	1.188E+00	2.898E-02
45.43	1.262E+00	2.4	1.470E-01	48.93	1.125E+00	2.689E-02
45.93	1.181E+00	2.4	1.434E-01	49.45	1.054E+00	2.522E-02
46.43	1.203E+00	2.3	1.522E-01	49.99	1.075E+00	2.490E-02
47.00	1.292E+00	3.9	1.712E-01	50.59	1.156E+00	4.475E-02
47.50	1.110E+00	3.7	1.530E-01	51.12	9.935E-01	3.700E-02
48.00	1.116E+00	3.4	1.600E-01	51.65	1.000E+00	3.432E-02
48.50	1.195E+00	3.6	1.782E-01	52.17	1.073E+00	3.907E-02
48.89	1.300E+00	4.6	1.997E-01	52.59	1.167E+00	5.367E-02
49.39	1.099E+00	4.3	1.755E-01	53.11	9.884E-01	4.225E-02
49.89	1.111E+00	3.9	1.841E-01	53.64	9.998E-01	3.873E-02
50.50	1.272E+00	4.1	2.206E-01	54.28	1.146E+00	4.731E-02
51.00	1.139E+00	4.2	2.050E-01	54.81	1.028E+00	4.285E-02
51.50	1.001E+00	4.7	1.870E-01	55.34	9.047E-01	4.207E-02
52.00	1.170E+00	5.7	2.264E-01	55.87	1.058E+00	5.993E-02
52.50	8.683E-01	5.7	1.741E-01	56.39	7.862E-01	4.475E-02
53.00	8.483E-01	4.1	1.762E-01	56.92	7.690E-01	3.166E-02
53.29	8.321E-01	3.9	1.764E-01	57.22	7.548E-01	2.923E-02
53.50	8.387E-01	5.0	1.804E-01	57.44	7.611E-01	3.831E-02
54.00	6.480E-01	5.9	1.443E-01	57.97	5.888E-01	3.494E-02
54.45	6.842E-01	3.1	1.571E-01	58.45	6.224E-01	1.941E-02
55.90	5.977E-01	5.1	1.512E-01	59.96	5.456E-01	2.766E-02
56.40	6.644E-01	4.4	1.736E-01	60.48	6.072E-01	2.701E-02
57.40	5.171E-01	5.6	1.441E-01	61.53	4.737E-01	2.661E-02
57.93	4.428E-01	4.6	1.276E-01	62.08	4.062E-01	1.877E-02
59.50	3.950E-01	6.8	1.256E-01	63.73	3.638E-01	2.491E-02
61.00	4.121E-01	5.9	1.434E-01	65.29	3.810E-01	2.267E-02
62.89	3.175E-01	7.2	1.233E-01	67.26	2.950E-01	2.113E-02
64.50	2.501E-01	7.5	1.063E-01	68.93	2.334E-01	1.748E-02
66.00	2.043E-01	8.8	9.426E-02	70.48	1.913E-01	1.687E-02
67.50	1.829E-01	8.6	9.137E-02	72.03	1.720E-01	1.479E-02
69.39	1.045E-01	9.9	5.753E-02	73.98	9.878E-02	9.804E-03
71.00	9.639E-02	9.5	5.750E-02	75.64	9.154E-02	8.652E-03
72.50	6.490E-02	12.5	4.163E-02	77.18	6.189E-02	7.725E-03
74.00	5.357E-02	12.5	3.687E-02	78.71	5.130E-02	6.406E-03
75.89	3.351E-02	16.5	2.514E-02	80.65	3.227E-02	5.324E-03
77.50	3.666E-02	14.6	2.954E-02	82.29	3.547E-02	5.171E-03
79.00	3.103E-02	17.1	2.666E-02	83.81	3.015E-02	5.167E-03
80.50	1.779E-02	21.0	1.628E-02	85.34	1.737E-02	3.646E-03
81.89	9.369E-03	29.5	9.075E-03	86.74	9.181E-03	2.706E-03
83.50	1.416E-02	22.1	1.462E-02	88.37	1.394E-02	3.086E-03
85.00	8.654E-03	30.3	9.471E-03	89.88	8.559E-03	2.591E-03
86.50	9.036E-03	27.3	1.046E-02	91.39	8.976E-03	2.452E-03
90.25	7.639E-03	30.3	1.013E-02	95.15	7.674E-03	2.329E-03
95.25	2.363E-03	73.2	3.701E-03	100.13	2.409E-03	1.763E-03